



Contents lists available at SciVerse ScienceDirect

## Global and Planetary Change

journal homepage: [www.elsevier.com/locate/gloplacha](http://www.elsevier.com/locate/gloplacha)

## Paleoceanographic conditions following the end-Permian mass extinction recorded by giant ooids (Moyang, South China)

Fei Li <sup>a,b</sup>, Jiaxin Yan <sup>a,\*</sup>, Thomas Algeo <sup>a,c</sup>, Xia Wu <sup>b</sup>

<sup>a</sup> State Key Laboratory of Biogeology and Environmental Geology, China University of Geosciences, Wuhan 430074, China

<sup>b</sup> Institute of Karst Geology, Chinese Academy of Geological Sciences, Guilin 541004, China

<sup>c</sup> Department of Geology, University of Cincinnati, Cincinnati, OH 45221-0013, USA

### ARTICLE INFO

#### Article history:

Received 8 April 2011

Received in revised form 10 September 2011

Accepted 26 September 2011

Available online xxx

#### Keywords:

Early Triassic

South China

anachronistic facies

giant ooids

carbonate fluorapatite (CFA)

### ABSTRACT

Early Triassic oceans were characterized by deposition of a number of “anachronistic facies”, including microbialites, seafloor carbonate cement fans, and giant ooids. Giant ooids were particularly prevalent in Lower Triassic sections across South China and exhibit unusual features that may provide insights into marine environmental conditions following the end-Permian mass extinction. The section at Moyang (Guizhou Province) contains abundant giant ooids ranging in size between 2 and 6 mm (maximum 12 mm) and exhibiting various cortical structures, including regular, deformed, compound, regenerated and “domed”. Preservation of ooid cortical structure is generally good as indicated by petrographic observations, and trace element and carbon isotope analyses suggest that diagenesis occurred in a closed diagenetic system. All ooids exhibit fine concentric laminae, frequently alternating between light-colored coarsely crystalline and dark-colored finely crystalline layers probably reflecting variation in organic content or original mineralogy. Under scanning electron microscope, biomineralized filaments or biofilms and tiny carbonate fluorapatite (CFA) crystals are commonly found in the finely crystalline layers. We infer that the precipitation of CFA was related to adsorption of P via microbial activity on the surfaces of ooids following episodic incursions of deep waters rich in CO<sub>2</sub>, H<sub>2</sub>S and phosphate into shallow-marine environments. Giant ooid precipitation may have been promoted in shallow ramp settings during these events by increased watermass agitation and supersaturation with respect to CaCO<sub>3</sub>, as well as reduced carbonate removal rates through biotic skeletal formation. Spatio-temporal distribution data reveal that giant ooids were widespread in the Tethyan region during the Early Triassic, and that they were most abundant immediately after the end-Permian crisis and disappeared gradually as metazoans repopulated marine environments.

© 2011 Elsevier B.V. All rights reserved.

### 1. Introduction

The end-Permian mass extinction was the largest catastrophe for marine ecosystems during the Phanerozoic (Stanley and Yang, 1994), during which ~90% of skeletonized metazoan species died out (Erwin, 1993, 1994). The Early Triassic was an unusual period biotically due to the low diversity of marine invertebrate assemblages, the slowness of the benthic ecosystem recovery (Hallam, 1991; Hallam and Wignall, 1997), and the flourishing of microbial communities (e.g., Pruss and Bottjer, 2004; Xie et al., 2005; Xie et al., 2010). These biotic developments were accompanied by large-scale environmental disturbances, including massive volcanism (e.g., Kamo et al., 2003; Isozaki et al., 2007; Payne and Kump, 2007) and deep-water anoxia in the global ocean (e.g., Wignall and Twitchett, 1996; Isozaki, 1997; Hotinski et al., 2001; Kump et al., 2005). In the sedimentary record, the Lower Triassic

is characterized by the widespread re-appearance of a number of distinctive deposits that had largely disappeared from normal-marine settings after the Cambrian and that are therefore considered “anachronistic facies” (Sepkoski et al., 1991). These deposits include flat pebble conglomerates (Wignall and Twitchett, 1999; Pruss et al., 2006), microbialites (Schubert and Bottjer, 1992; Kershaw et al., 1999; Lehrmann, 1999; Pruss et al., 2006; Baud et al., 2007), wrinkle structures (Pruss et al., 2004; Mata and Bottjer, 2009) and seafloor carbonate cement fans (Woods et al., 1999, 2007) that developed in settings ranging from intertidal to basinal.

Carbonate ooids are widely distributed in the Lower Triassic of the Tethys Ocean region, including in southern Austria (Krainer and Vachard, 2009), Germany (Weidlich, 2007), Hungary (Hips and Haas, 2006), northern Italy (Baud et al., 1997; Fraiser et al., 2005), Turkey (Baud et al., 1989; Kershaw et al., 2010), Iran (Gaetani et al., 2009), and Oman (Ricoz et al., 2005). In the eastern Tethys, the peri-equatorial South China Craton also developed extensive carbonate ooid deposits following the end-Permian mass extinction (Fig. 1A). Due to their temporal association with the aftermath of the end-Permian mass extinction, they are regarded as “disaster deposits” (Groves et al., 2003). Lower Triassic

\* Corresponding author at: 388#, Lumo Road, Faculty of Earth Sciences, China University of Geosciences (Wuhan), Wuhan City, Hubei Province, China. Tel.: +86 27 67883504; fax: +86 27 67883456.

E-mail addresses: [feinan.li@gmail.com](mailto:feinan.li@gmail.com) (F. Li), [jxyan\\_cn@yahoo.com](mailto:jxyan_cn@yahoo.com) (J. Yan).

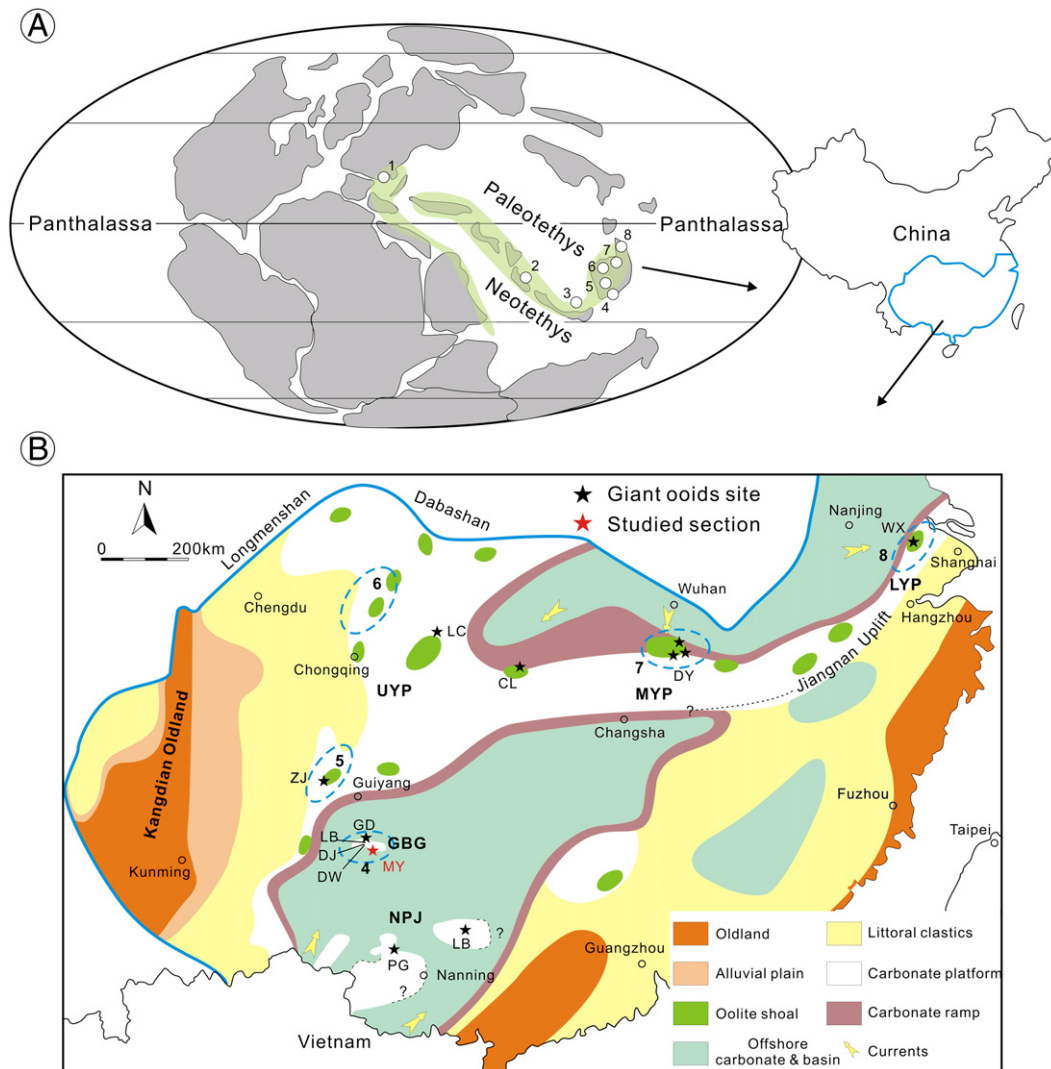


**Fig. 1.** A) Global paleogeography of Early Triassic with reported giant-oid deposits, including 1 Germany, 2 Qiangtang Block (northern Tibet), 3 Yidun Block, 4 Nanpanjiang Basin, 5, 6, 7 and 8 are four districts of giant-oid deposits in the Yangtze Platform. Light green zone shows distribution of oolitic sediments (see text in Section 1). B) Enlarged regional paleogeography of South China and the distribution of oolite shoals in the Early Triassic. Stars indicate localities that developed giant ooids: CL—Cili, DY—Daye, GD—Guandao, LB—Laibin, LC—Lichuan, MY—Moyang, PG—Pingguo, WX—Wuxi, and ZJ—Zhijin (see Fig. 2 for their lithostratigraphic correlation; also see Table 1, and references therein). Other features: GBG—Great Bank of Guizhou, NPJ—Nanpanjiang Basin, UYP—Upper Yangtze Platform, MYP—Middle Yangtze Platform, LYP—Lower Yangtze Platform, LB—Langbai, DJ—Dajiang and DW—Dawen. Map adapted from Feng et al. (1997) and Lehrmann et al. (2007).

ooids are unusual in their relatively large size, some being “giant ooids” (in this paper, we use the term “giant ooids” rather than “pisoids” to avoid any possible inference of a freshwater/terrestrial origin), i.e., evenly coated grains with diameters  $> 2$  mm, although they share many structural and mineralogical characteristics with the smaller ooids commonly found in both modern and ancient shallow-marine settings (Richter, 1983; Siewers, 2003; Flügel, 2004). Giant ooids were common in the Neoproterozoic but rare after the Cambrian (Sumner and Grotzinger, 1993; Trower and Grotzinger, 2010). Whether Early Triassic giant ooids were the product of environmental conditions similar to those prevailing during the Neoproterozoic is an issue currently under investigation.

A Lower Triassic oolite succession bearing giant ooids is well exposed in the Moyang section of Guizhou, South China. In a Chinese-language paper, we described the types and size variations of these carbonate ooids as well as their depositional features (Li et al., 2010). The present paper expands on this earlier work by (1) reporting the C- and O-isotopic, and trace-element compositions of these ooids, (2) offering a fuller analysis of their microfacies associations, and (3) proposing a new hypothesis linking their origin to unusual aqueous chemical conditions that were common in Early Triassic

marine environments. In this contribution, we also present a revised paleogeographic map of the South China block showing the distribution of Lower Triassic oolitic facies, as well as a detailed correlation table documenting their stratigraphic range of occurrence. Finally, we have compiled the occurrences of giant ooids through Earth history based on a literature search, in order to assist in identification of common environmental controls on their development.

## 2. Location and geological setting

### 2.1. Geological background

The South China block was located at peri-equatorial latitudes in the eastern Tethys Ocean during the Permian–Triassic (Fig. 1A). It is composed of the Yangtze Craton and the South China fold system, as well as the Nanpanjiang Basin (Sun et al., 1989) (Fig. 1B). The Yangtze Platform of the Yangtze Craton was tectonically stable and covered by an extensive succession of shallow-marine carbonates (Wu et al., 1994; Enos, 1995; Feng et al., 1997).

After a major transgression commencing in the latest Permian, the margin of the Upper Yangtze Platform retreated more than 100 km

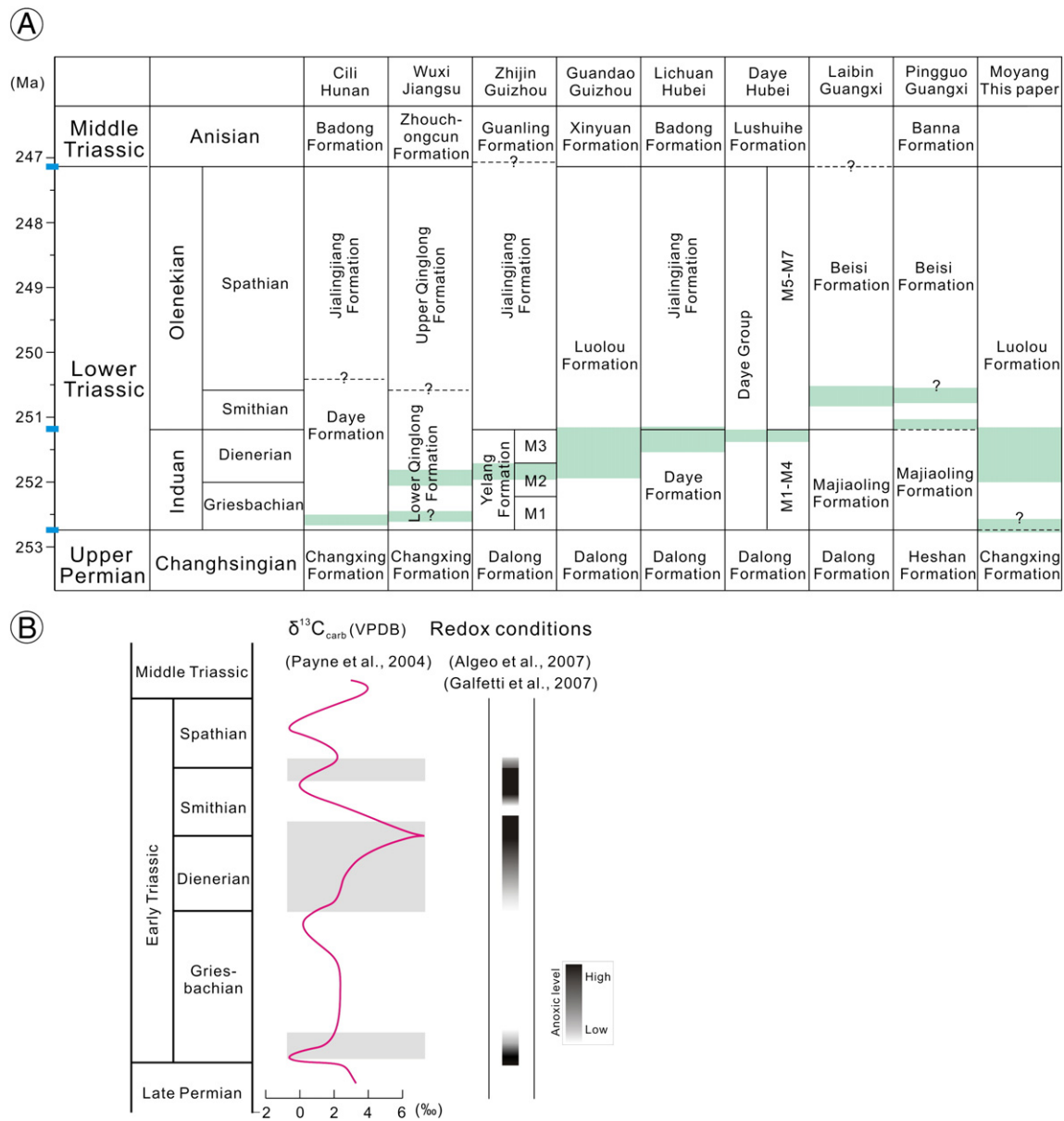


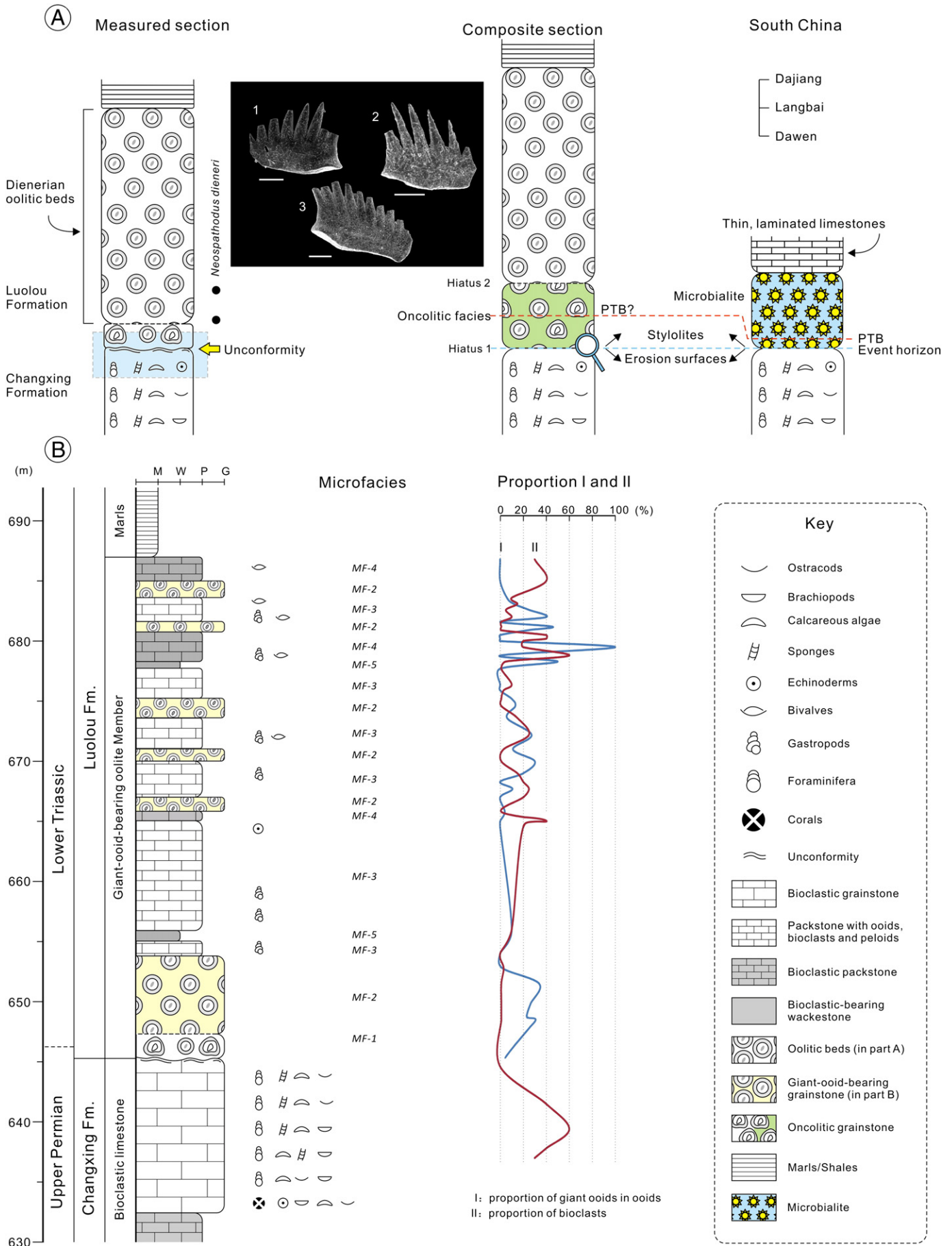
**Fig. 2.** (A) Diagram showing ages and lithostratigraphic units in Lower Triassic strata of South China. The time scale containing the Permian–Triassic boundary (252.6 Ma), the Induan–Olenekian boundary (251.2 Ma) and the Lower–Middle Triassic boundary (247.2 Ma) is from Mundil et al. (2004), Galfetti et al. (2007) and Lehrmann et al. (2006), respectively. The greenish zone in each column indicates the occurring range of giant ooids (compiled sections are from Li et al., 2010, and references therein). Abbreviation: M: Member. (B) Correlation of giant-oid occurrences (shaded) with  $\delta^{13}\text{C}$  curve of the Great Bank of Guizhou (Payne et al., 2004), and redox conditions in the Nanpanjiang Basin (Algeo et al., 2007; Galfetti et al., 2007) as determined from lithology (black, laminated, and organic-rich shale) and carbon isotopes.

northward, producing a huge carbonate ramp across the top of the platform in the earliest Triassic (Wu et al., 1994; Enos, 1995; Feng et al., 1997; Lehrmann et al., 2005). Ooid shoals were common in up-ramp settings, especially in a broad region to the east and south of the Kangdian Oldland (or Khamdian Massif). Meanwhile, oolitic facies expanded westward and northward until close to the edge of the Yangtze Craton in the regions of Longmenshan and Dabashan, respectively (Wu et al., 1994).

Deposition of oolite on the middle and lower Yangtze Platform was influenced by the Jiangnan Uplift (Wu et al., 1994), a shallowly submerged topographic high on the southern border of the Yangtze Craton. Uplift of this feature resulted in its evolution from a platform margin with framework reefs and bioclastic shoals in the Late Permian to a low-angle ramp with oolite shoals in the Early Triassic (Wu et al., 1994). The gradual progradation of the oolite shoal facies on the upper ramp lasted until the beginning of the Smithian substage

(Olenekian Stage, Early Triassic) in the western part of the middle and lower Yangtze Platform, and probably until the Spathian substage (Olenekian Stage) in the eastern part of the platform (Zhu et al., 1986; Zhu, 1992).

The Nanpanjiang Basin is a deep-water embayment on the southern margin of the South China block within which several isolated carbonate platforms developed during the Early Triassic on the foundations of older (Late Permian) platforms (Lehrmann, 1999; Lehrmann et al., 2005). However, the foundation of the Great Bank of Guizhou (GBG) differs in having been inherited from a portion of the Late Permian Yangtze Platform reef margin (Lehrmann, 1993, 1999; Lehrmann et al., 2005). In the low-relief bank stage of carbonate platform development, calcimicrobial framestone of earliest Triassic age was deposited on Upper Permian skeletal grainstone. Subsequently, oolite shoals developed locally around the platform margin and occasionally extended across the entire platform during the Early Triassic (Lehrmann, 1999;



Payne et al., 2006a). Giant ooids are found in oolitic shoal facies on the margins of the Yangtze Platform as well as on isolated carbonate platforms of the Nanpanjiang Basin (Fig. 2A).

## 2.2. Study area

The Moyang study section is located on the southern margin of the GBG (Fig. 1B). The section is located near Moyang village, 0.6 km north of the new Moyang town, in Luodian County, Guizhou Province. The outcrop is along the road connecting Dongdang and Moyang towns. The section consists of a ~690-m-thick carbonate-dominated succession of Middle Permian to Lower Triassic age, including (in ascending order) the Permian Qixia (Chihhsia), Maokou, Wujiaping, and Changxing formations and the Lower Triassic Luolou Formation. Dark gray, thin- to medium-bedded cherty limestone of the upper Maokou Formation of Middle Permian age is overlain by thick-bedded bioclastic limestone of the Wujiaping Formation of early Late Permian age. The late Late Permian Changxing Formation consists of massive, gray bioclast-rich limestone, with highly diverse shallow-marine invertebrate faunal communities (Fig. 3). Microscopic observation reveals that Changhsingian microfacies consist mainly of skeletal grainstone containing bioclasts of *Tubiphytes*, sponges, foraminifers, rugose corals, gastropods, echinoderms, and brachiopods. Where reef boundstone is present in the uppermost Changxing Formation, sphinctozoan sponges and *Archaeolithoporella* as well as early marine cements comprise the framework (Fig. 4A and B). The base of the Luolou Formation consists of an oncolitic unit (from 0 to 60 cm thick) overlain by oolitic beds (from 2 to 40 m thick) that can laterally traced over ~500 m, then conformably thinning rapidly eastward (Fig. 4A). The oncolitic facies consists of dark-gray grainstone containing oncoids with variational sizes (0.5–5 mm) and uneven laminae, minor ooids (including some giant ooids; partly with dissolved sharps), and rare fossil debris. Above the basal oncolitic and oolitic beds, the Lower Triassic Luolou Formation consists mainly of thin-bedded purplish marls.

## 2.3. Age and stratigraphic relationships

Biostratigraphic identification of the Permian–Triassic boundary (PTB) is not well-developed for Moyang. Previously, the PTB at Moyang was placed at the contact between the oolitic facies and the overlying marls of the Luolou Formation, making the oolitic beds uppermost Permian in age (Tian and Zeng, 1995; Jin, 1997). However, the conodont fossil *Neospathodus dieneri* has been found at the base and in the lower part of the oolitic beds, revising their age to the Dienerian substage (Induan Stage, Early Triassic; Fig. 3A). The underlying oncolitic facies, comprising the basal beds of the Luolou Formation, contains no age-diagnostic fossils. This facies is separated from the bioclastic grainstone and sponge boundstone of the Late Permian Changxing Formation by an unconformity marked by stylolites and an erosion surface, demonstrating the existence of at least a minor hiatus at the Changxing–Luolou formation contact (Figs. 3A and 4C–F).

A hiatal contact marked by stylolites and erosion is present in many Permian–Triassic sections of the GBG, in some of which the taxon diagnostic of the PTB (the conodont *Hindeodus parvus*; Yin et al., 2001) has been identified within the calcimicrobial facies above the contact (e.g., Kershaw et al., 2007; Liu et al., 2007; Payne et al., 2007; Collin et al., 2009; Yang et al., 2011). Based on their similar character, we suggest that the hiatus at the base of the oncolitic facies

in Moyang overlaps in age those at the base of the calcimicrobial facies in other GBG sections. These considerations suggest that the PTB is located either within or at the top of the oncolitic facies at Moyang, although further biostratigraphic work is needed to define the exact timing. A second hiatus, equivalent to most or all of the Griesbachian substage of the Induan Stage of the Early Triassic, is thus likely to be present between the basal oncolitic facies and the overlying oolitic beds of the Luolou Formation (see Fig. 3A). The documented Dienerian age of the giant-oid-bearing oolites at Moyang are comparable with an oolitic facies of the same age in the Guandao section on the northern margin of the GBG (Figs. 1A and 2A; Payne et al., 2006b).

## 3. Methods and materials

Detailed petrographic and microfacies examinations were conducted on thin sections at a resolution of at least one sample every meter through the study section. Geochemical analysis was conducted by electron probe microanalysis (EPMA; JXA-8100) on polished and conductively (carbon) coated samples, with a detection limit of 100 ppm. The oxides of Na, Ca, C, Mn, Mg, P, Fe, Si, S and Sr were determined in this study. A scanning electron microscope (SEM; Quanta 200) with energy dispersive spectrometer (EDS) was used to examine the microstructure of ooid cortices. Some slab surfaces for SEM analysis were initially etched in 5% HCl for 5–15 s (or etched in dilute acetic acid solution for 10 s as a contrast), then washed with water, dried, and coated with gold. Sample preparation and analytical techniques follow guidelines of *Dahanayake and Krumbein (1985) and Folk (1993)*. Sample powders for  $\delta^{13}\text{C}$  (VPDB) and  $\delta^{18}\text{O}$  (VPDB) analyses were collected from fresh ooid cortices (mixed with nuclei material) and the sample matrix (outside of ooids), then determined by analyzing  $\text{CO}_2$  generated through reaction of the sample with 100% phosphoric acid (McCrea, 1950) on a MAT-251 IR-MS. All geochemical analyses were carried out in the State Key Laboratory of Geological Processes and Mineral Resources at the China University of Geosciences (Wuhan). In order to examine the temporal distribution of giant ooids, we tabulated their age, location, maximum size, and depositional environment from literature reports (Table 1).

## 4. Results

### 4.1. Petrography and microfacies

The Moyang ooids examined in the field display a size-distribution mode between 2 and 6 mm, and maximum diameters ranging up to 12 mm (Fig. 4G). The main types observed include regular ooids, deformed ooids, compound ooids, broken ooids, regenerated ooids, and “domed ooids” (details in Table 2). Ooid nuclei generally consist of granular calcite grains, peloids, ooid fragments, and small ooids. Most of the granular calcite grains may have been composed of aragonitic fossil fragments originally, such as gastropods and bivalves.

The giant-oid-bearing oolite member (comprising oncolitic and oolitic beds) of the Luolou Formation contains five microfacies types from which relative sea-level changes can be reconstructed (see Fig. 5 and Table 3). In the lower part of the oolite member, giant-oid-bearing oolite and oncolite (*MF-1* and *MF-2*) are dominant, representing a high-energy shoal environment. Upsection, the percentage of ooids gradually declines and bioclastic wackestone (*MF-5*) becomes dominant, suggesting deepening to relatively low-energy subtidal

**Fig. 3.** (A) Columns of studied sections at Moyang, showing age, stratigraphic relationships, and correlations with microbialite-bearing PTB sections of the Great Bank of Guizhou. Note that the eroded and stylolitized contact at the base of the oncolitic facies at Moyang is similar to that found at Dajiang (Yang et al., 2011), Langbai (Payne et al., 2007; Collin et al., 2009), and Dawen (Liu et al., 2007). The position of the PTB is uncertain but constrained by the stratigraphically lowest occurrences of the Dienerian conodont *Neospathodus dieneri* (SEM photos of conodonts from the oolitic beds; bar scale = 100  $\mu\text{m}$ ). (B) Moyang stratigraphic data: measured stratigraphic column, main fossils, microfacies types, and two curves showing frequency of giant ooids and bioclasts. Ooid and bioclast frequency data based on thin-section point counts; note the inverse frequency relationship of these curves, especially in the 675–685 m interval.

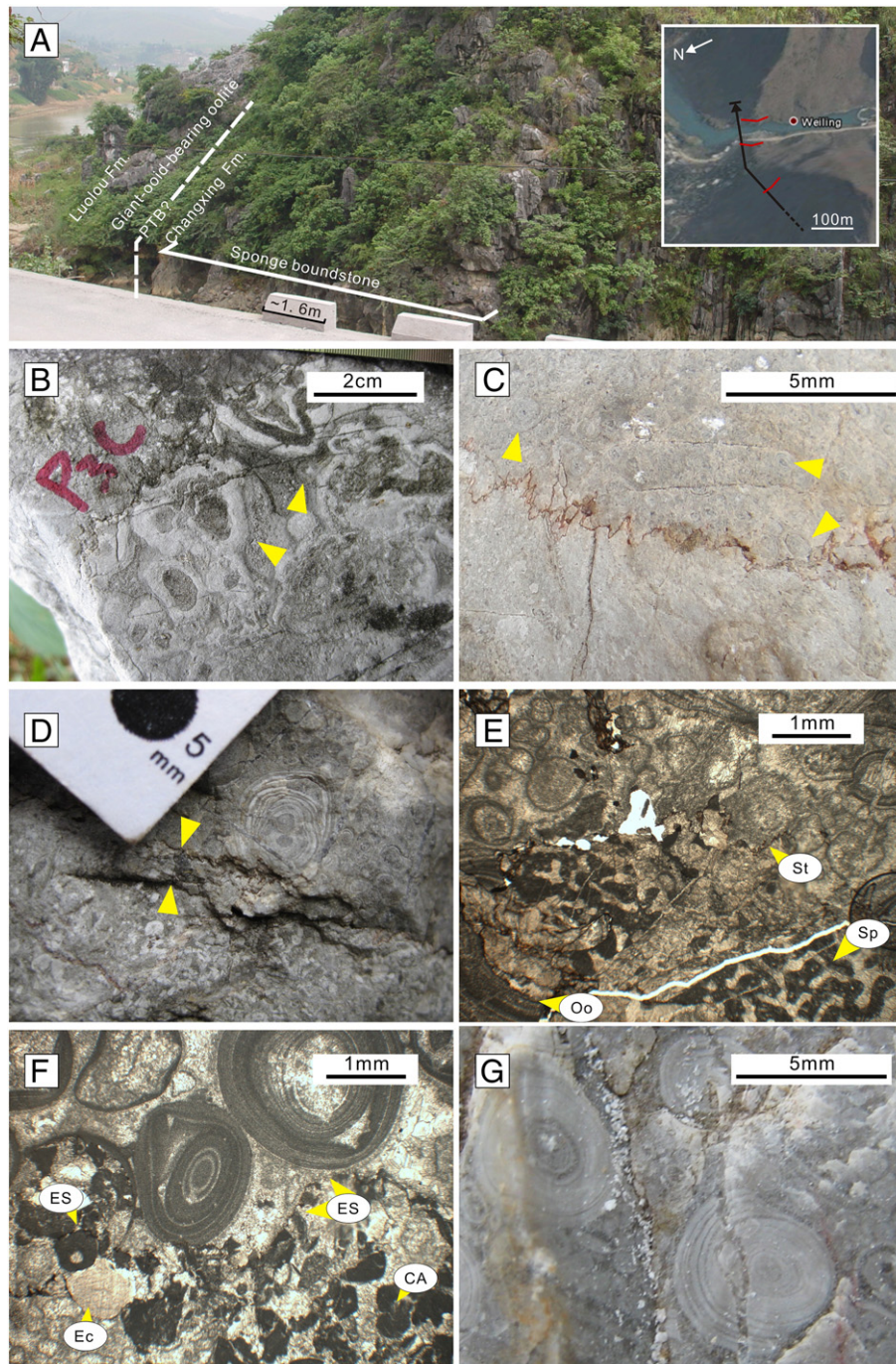


**Fig. 4.** Photographs of the Permian–Triassic boundary and giant ooids at Moyang section, Guizhou. (A) Outcrop photograph showing the PTB. Satellite imagery (from the Google Earth) in the right box presents the outcrops of Moyang (red lines), and a 2 to 40 m thick giant-oid-bearing oolitic beds can be laterally traced over ~500 m (black line). (B) Calcareous algal-sponge boundstone and early marine cements (yellow arrows) comprise the framework of the Changxing Formation. (C) A stylolite separates Changhsingian sponge boundstone and oncolitic facies including giant ooids (yellow arrows; latest Permian?). (D) Two erosion surfaces (yellow arrows) along the contact between uppermost Permian bioclastic grainstone and overlying oncolitic grainstone. (E) Thin section view of (C). (F) Thin section view of one erosion surface in the latest Permian. Note two distinct facies separated by a thin erosion surface. (G) Fresh surfaces of giant-oid-bearing oolite. Note that smooth concentric laminae differentiate giant ooids from other coated grains. Abbreviations: CA: calcareous alga; Ec: echinoderm; ES: erosion surface; Fm.: Formation; Oo: ooid; Sp: sponge; St: stylolite. (For interpretation of the references to color in this figure legend, the reader is referred to the web version of this article.)

environments. Subsequently, the percentage of ooids rises again, and mixed bioclastic–oolitic grainstone (*MF-3*) become dominant, reflecting a shallowing trend. In the upper half of the oolite member, oolitic grainstone and bioclastic–oolitic packstone occur alternately, suggesting frequent variation between high-energy intertidal and moderate-energy subtidal facies. In the uppermost part of the oolite member, the percentage of ooids drops sharply and bioclasts (mostly bivalves) regain dominance (*MF-4* to *MF-5*).

The microfacies documented in this study are similar to those of earlier studies of the GBG (Payne et al., 2006a) and Pingguo Platform (Lehrmann et al., 2007). Packstone–grainstone beds containing mixtures of ooids and micro-gastropods (*MF-3* and *MF-4*) can be compared with the age-equivalent Gastropod Oolite Member of the Werfen Formation in northern Italy (Posenato, 2008), which has been interpreted to record a prolonged interval of chemically and/or physiologically harsh conditions in a shallow-marine environment

**Table 1**  
Occurrences of giant-ooids from shallow-marine environments in geological records.

Time	Location	Size (Max)	Environment	References
Late Archean	Carawine Dolomite., Australia	Up to 6 mm	Low energy platform	(Simonson et al., 1993)
Late Archean	Boomploas Fm., South Africa	Up to 5 mm	Platform-edge	(Beukes, 1983)
Late Archean	Reivilo Fm., South Africa	Up to 3 mm	Ramp	(Sumner and Grotzinger, 1993)
Late Archean	Frisco Fm., South Africa	Up to 18 mm	Rimmed shelf/lagoon	(Sumner and Grotzinger, 1993; Sumner, 1997)
Paleoproterozoic	Transvaal Dolomite, South Africa	Up to 2.6 mm	–	(Truswell and Eriksson, 1973)
Paleoproterozoic	Rocknest Fm., Northwest Canada	Up to 2.5 mm	Back reef/lagoon	(Grotzinger and Reed, 1983; Sumner and Grotzinger, 1993)
Mesoproterozoic	Siyeh–Snowslip Fm., Montana	Up to 2.5 mm	Shallow-marine shelf	(Tucker, 1984)
Neoproterozoic	Beck Spring Fm., California	Up to 10 mm	Ramp	(Zempolich et al., 1988; Corsetti et al., 2006; Trower and Grotzinger, 2010)
Neoproterozoic	Grainstone Fm., Northwest Canada	Up to 10 mm	Inner ramp	(Batten et al., 2004)
Neoproterozoic	Katakaturuk Dolomite., Alaska	Up to 10 mm	Shelf margin	(Clough and Goldhammer, 2000)
Neoproterozoic	Eleonore Bay Group, Greenland; Backlundtoppen Fm., Svalbard	Up to 14 mm	Ramp/Shallow marine	(Swett and Knoll, 1989)
Neoproterozoic	Trezona Fm., South Australia	Up to 16 mm	Subtidal barrier?	(Singh, 1987)
Neoproterozoic	Yellowhead Platform, Alberta	Up to 4.5 mm	Ramp	(Teitz and Mountjoy, 1988)
Neoproterozoic	Wilhite Fm., Smokey Mountains	Up to 5 mm	–	(Sumner and Grotzinger, 1993)
Neoproterozoic	Wyman Fm., California	Up to 8 mm	Shallow water	(Zenger, 1976)
Neoproterozoic	Keele Fm., Northwest Canada	Up to 5 mm	Inner Ramp	(Day et al., 2004)
Neoproterozoic	Johnnie Fm., California	Up to 12 mm	Shallow marine	(Sumner and Grotzinger, 1993; Trower and Grotzinger, 2010)
Late Cambrian	Riley Fm., Texas	Up to 8 mm	Ramp?	(King and Chafetz, 1983)
Late Cambrian	Warrior Fm., Pennsylvania	Up to 16 mm	Tidal channel?	(Heller et al., 1980)
Late Cambrian	Nolichucky Fm., Virginia	Up to 4 mm	Shallow ramp	(Markello and Read, 1981)
Late Cambrian	the Port au Port Group, Canada	Up to 4 mm	Shallow subtidal environment	(Chow and James, 1987)
Latest Ordovician	Keel Fm., Oklahoma	Up to 5 mm	Shallow seaways	(Amsden and Barrick, 1986)
Late Silurian	Pipe Creek Junior Reef, Indiana	Up to 16 mm	Shallow marine	(Frank et al., 1993)
Carboniferous	Lower Tournaisian, Velbert, Germany	0.5–6 mm	Shelf	(Flügel, 1982; Bates and Brand, 1990)
Carboniferous	Upper Pennsylvanian, Plattsburg Limestone, Kansas	Up to 3 mm	Open marine	(Wilkinson et al., 1984)
Early Triassic	Moyang, South China	Up to 12 mm	Ramp	(Li et al., 2010; and references therein)
	Cili, South China	Up to 4 mm		
	Daye, South China	1–8 mm		
	Zhijin, South China	>2 mm		
	Laibin, South China	5–8 mm		
Early Triassic	Lichuan, South China	1–5 mm	Ramp	(Mei, 2008)
Early Triassic	Wuxi, South China	>2 mm	Ramp	(Tang, 1987; Y. Wang, personal communication, 2010)
Early Triassic	Guandao, South China	Up to 10 mm	Low-rift platform	(Payne et al., 2006b)
Early Triassic	Pingguo, South China	5–10 mm	Low-rift platform	(Lehrmann et al., 2007)
Early Triassic	Yingshuiquan Fm., Shuanghu, Qiangtang	Up to 5 mm	–	(Zhu et al., 2005)
Early Triassic	Cigang Fm., Western Sichuan (Yidun Block)	>2 mm	platform-margin	(Regional Geological Survey of Sichuan Bureau of Geology and Nanjing Institute of Geology and Palaeontology, 1982)
Early Triassic	Rogenstein Member, Germany	Up to 20 mm?	Shallow water	(Weidlich, 2007)
Early Jurassic	Upper Lias, Central England	Up to 3 mm	Shallow water	(Horton et al., 1980)
Middle–Late Jurassic	Vajont Limestone, Italy	>2 mm (size from photo)	Unprotected windward platform-margin	(Bosellini et al., 1981)
Late Jurassic	Oolithe corallienne de Pagnoz Fm., French	Up to 2.2 mm (concentric)/Up to 2.7 mm (micritic)	Shoal (shelf)	(Reolid et al., 2007)
Late Jurassic	Upper Tithonian, Croatia	1–3 mm	–	(Husinec and Read, 2006)

(Fraiser et al., 2005). The two curves in Fig. 3B show that (a) giant ooids are most abundant in oolitic beds containing few or no bioclasts; and (b) both regular-sized and giant ooids decrease in abundance as the proportion of bioclasts increases and bivalves become more common in the upper part of the oolite member (Fig. 5E). These observations suggest that the growth environment of giant ooids was generally not conducive to living metazoans.

#### 4.2. Microstructure

Plain-light petrography examination show ooid cortices are composed of distinct, alternately light- and dark-colored laminae, both of which are smooth layers having regular boundaries (Fig. 6). All laminae are now composed of low-Mg calcite, but crystal size differs between the laminae under the polarizing microscope, being coarser for light-colored laminae and finer for dark-colored laminae (Fig. 6C and E).

Note that when under the SEM, the bright laminae comprise of fine grains (typically 4–8  $\mu\text{m}$ ) but containing strong electronic imaging, and probably corresponding to the dark-colored laminae (Fig. 7B–D).

The intergranular cements between ooids are bladed calcites that exhibit broad flattened and pyramid-like terminations and average about 10  $\mu\text{m}$  in width and 20–90  $\mu\text{m}$  in length (Fig. 7). The bladed cement forms thin isopachous fringe around ooids (Fig. 7A). A second generation of cement that fills the remaining space between ooids consists of blocky calcite crystals ranging in size from 15  $\mu\text{m}$  to hundreds of microns.

SEM examination of polished samples shows an abundance of small, scattered non-carbonate mineral grains that are integrated within the concentric fabric of ooid laminae (Fig. 7E). These grains are found in association mainly with the brightly and finely crystalline ooid laminae, often as a large number of grains concentrated along a single ooid lamina surface. The elemental composition of this mineral phase is given in

**Table 2**  
Major types of ooids from Moyang section.

Ooid type	Description	Abundance	Environment
Regular ooid	The distribution of size variation is approximately normal. Spheroidal–ellipsoidal shape. Smooth concentric cortices, alternately light- and dark-colored laminae. 1) The light-colored laminae with coarsely sparitic texture and the dark-colored laminae with fine carbonate crystals in association with abundant organic substrates; 2) Also some comprise conspicuously black colored laminae, may indicate incorporation of organic matter. Gastropods as the main associated fossils.	High	High-energy
Deformed ooid	Ooids are distinctly stretched or flattened, indicating tectonic stress result in plastic deformations.	Low	Diagenesis
Compound ooid	Mostly ellipsoidal shape. Multiple small ooids bounded together, then circum-coated. Intergranular sparitic calcite crystals occupying the remaining of nuclei. The cortices consist of alternately light- and dark-colored laminae, and outer laminae are more regular than inner.	Low	Medium- to low-energy
Broken ooid	1) Fragment of concentric ooid (mostly are ruptured outer cortical layers); 2) Partly cracked ooid (indicate dissolution of internal laminae or shallow burial compaction). Occurring together with regular ooids and regenerated ooids.	Abundance in the base of Oolite Member, other is low.	High-energy/diagenesis
Regenerated ooid	1) Broken ooid as nucleus surrounded by thin laminae; 2) small ooids act as nuclei develop in multi-stage process which can identified by alternative cortical thickness and density	Medium	High-energy
Domed ooid	Outer cortices exhibit domed shape, without stretched or broken features. Resembles “pendant cements”, but intergranular cements do not show similar features. The direction of doming of ooid cortices is non-oriented. Associated with compound ooids.	Rare, found in a single sample.	Not clear

**Table 4.** Both the CaO:P<sub>2</sub>O<sub>5</sub> ratio and F content (mean 3.5 wt.%; from EDS) of the mineral are in agreement with the mineral being carbonate fluorapatite (CFA), after the empirical formula Ca<sub>5</sub>(PO<sub>4</sub>)<sub>2.5</sub>(CO<sub>3</sub>)<sub>0.5</sub>F (corresponding to Ca = 41.16%, P = 15.91%, C = 1.23%, O = 37.79% and F = 3.90% by weight) (from McClellan and Van Kauwenbergh, 1990). When etched with 5% HCl, the internal structure of the cortex reveals that the CFA is present as a cluster coating on clay minerals (probably illite; Fig. 8). This demonstrates that the CFA precipitated after uptake of illite on the growing ooid surface, with the illite acting as a substrate for CFA precipitation during early diagenesis. Formation of CFA may have resulted from adsorption of dissolved phosphate onto illite crystals (e.g., due to interaction of phosphate with metallic cations on clay-mineral surfaces) that have a high adsorptive capacity and adhered to ooids on the seafloor environment (Edzward et al., 1976; Krom and Berner, 1980).

SEM examination also reveals that ooid cortices contain a variety of microbial fabric types, including filamentous networks and biofilms particularly in the finely crystalline laminae (Fig. 9C and D). Microbial filaments are tiny elongated tubes with diameters ranging from 1 to 10 μm that occupy intercrystalline space in ooid cortices. Some filaments exhibit small calcite crystals that have developed on their depressed surfaces (Fig. 9E). This relationship implies an in situ origin for these filaments, demonstrating that they are probably filamentous cyanobacteria in origin (Davaud and Girardclos, 2001; Plee et al., 2008). In addition, some ooids preserve biofilms covering internal lamina surface with their cortices that, in some instances, served as a substrate for diagenetic growth of granular CFA mineral clusters (Fig. 9F and G).

#### 4.3. Geochemistry

Sr–Mn covariation can provide information about the degree of diagenetic alteration of carbonate samples, and Sr concentrations can assist in interpreting the original mineralogy of ooid cortices. The Sr content of giant ooids in this study ranges from 558 to 1234 ppm (average 786 ppm), and the Mn content averages less than 200 ppm (Fig. 10). Uniformly low Sr concentrations are consistent with a primary calcite mineralogy for the ooids (see Section 5.1). Mn concentration of carbonate minerals varies mainly as a function of diagenetic alteration: primary calcite and aragonite generally contain <50 ppm Mn but secondary carbonate mineral phases that have formed under reducing (burial) conditions can contain much higher

Mn concentrations. The distribution of Moyang samples on a Sr–Mn crossplot (Fig. 10) implies that the samples with low Mn experienced only limited diagenetic alteration whereas those with high Mn values experienced greater alteration.

Na concentrations have been used as a possible paleosalinity indicator in ancient carbonates (Veizer et al., 1977; Tucker, 1985). The average Na concentration in the study samples is 215 ppm, close to the threshold value for hypersaline conditions (230 ppm). However, relying solely on Na to interpret marine salinity is debated (Flügel, 2004). The presence of stenohaline, normal-marine fossils (such as echinoderms) in adjacent strata provides evidence of a non-hypersaline shallow-marine environment. No micro-dolomite or high-Mg content is present to suggest that the original mineralogy of Moyang giant ooids was high-Mg calcite. The concentrations of Fe and related metallic elements were used to examine whether iron compounds (i.e., chamosite and glauconite) exist in ooid cortices (Fig. 9H). In addition, the Si content probably reflects the presence of phyllosilicate minerals such as illite, which are ubiquitous in small quantities in the Moyang section.

Stable carbon and oxygen isotope analysis of the giant ooids (Fig. 11) reveals that δ<sup>13</sup>C values (VPDB) vary from 1.61‰ to 2.65‰, and δ<sup>18</sup>O values (VPDB) range from –6.72‰ to –4.57‰. Matrix samples (interparticle cements; colored in Fig. 11) have similar δ<sup>13</sup>C values but slightly heavier δ<sup>18</sup>O values. Marine carbonate C-isotope curves for the Early Triassic show that most formations yield δ<sup>13</sup>C values between –2‰ and +4‰ (Baud et al., 1989; Veizer et al., 1999; Corsetti et al., 2005; Korte et al., 2005; Korte and Kozur, 2010), although Dienerian strata from the GBG yield δ<sup>13</sup>C values ranging from 1‰ to 8‰ (Payne et al., 2004). The C-isotope data presented here are consistent with these previous studies and imply minimal alteration of Moyang giant ooids. In contrast, lighter C-isotopic compositions are shown by giant-ooid samples approximately contemporaneous with that at Moyang in the Dienerian substage from the Lower Triassic (Bernburg Formation) of the Germanic Basin (between –1‰ and +1‰; see Fig. 10; Weidlich, 2007, 2010). Whether the isotopic compositions of the latter units are due to unusual environmental conditions or to greater diagenetic influence is uncertain at present. The O-isotopic compositions of Moyang giant ooids are close to those inferred for primary marine carbonates of Early Triassic age (Veizer et al., 1999; Richoz et al., 2010), although probably they have been reset during diagenesis (cf. Brand and Veizer, 1981; Veizer, 1983).

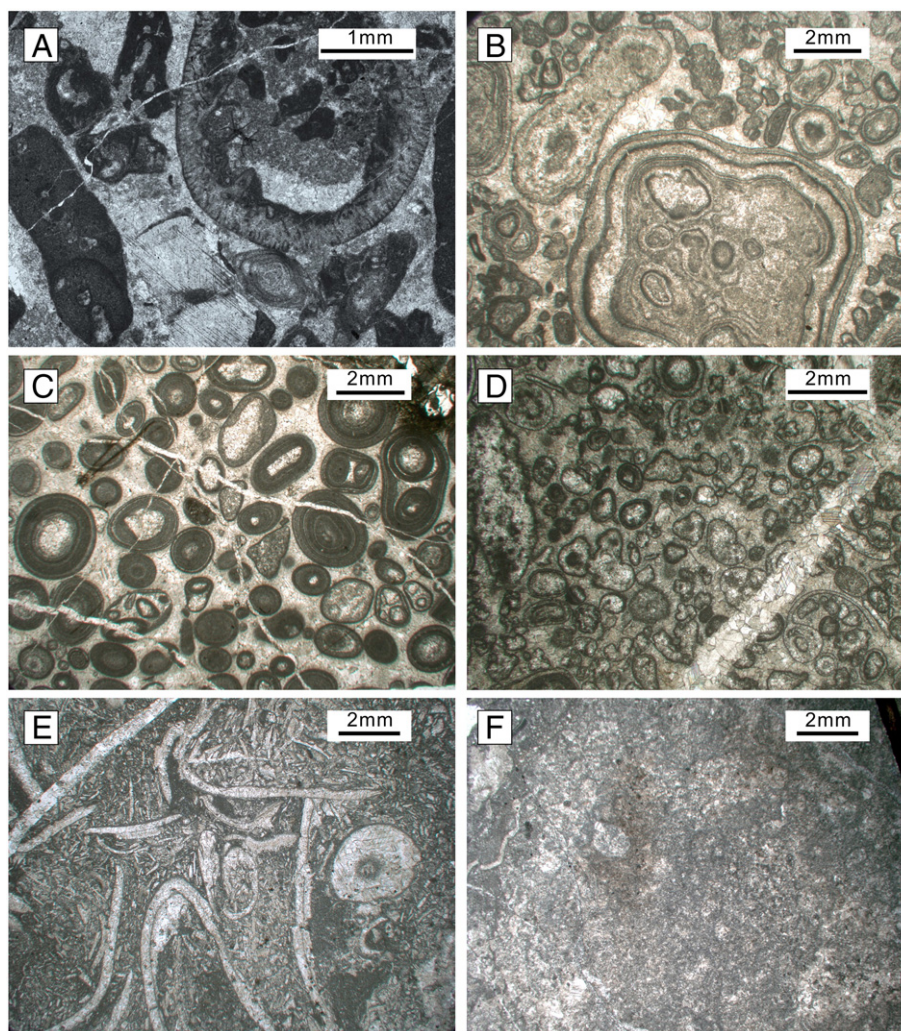


**Fig. 5.** Microfacies types. (A) Skeletal grainstone in Changxing Formation. (B)–(F) are MF-1, MF-2, MF-3, MF-4 and MF-5, respectively. See Table 3 for a detailed description of microfacies.

**Table 3**  
Microfacies and depositional environments from the Moyang.

Microfacies type	Description	Fossils	Environment
MF-1 Oncolitic grainstone	Well-sorted grainstone, oncoids dominant, minor amounts of ooids. Oncoids have broad and irregular shapes, some have overlapping laminae.	Rare bioclasts	Shallow subtidal
MF-2 Giant-oid-bearing oolitic grainstone	Well-sorted oolitic grainstone, abundant ooids with concentric laminae. A few oncoids with elongate shapes, and fine peloids locally abundant. Dominant ooid nucleus type is granular calcite grains, and intergranular cements are comprised of bladed and blocky calcites. Peloids are locally abundant.	Rare bioclasts except few gastropods	Ooid shoal, high energy, winnowing by wave and/or storms.
MF-3 Oolite-gastropod grainstone	Dominated by ooids and gastropods, minor other bioclasts and peloids. Except normal ooids, other types are various, including deformed ooids, compound ooids, regenerated ooids and few "domed ooids". Some ooids nearly micritized, and some bioclasts have micritic envelopes.	Gastropods dominant, from 1 to 2 mm in size, spines sometimes preserved. Some echinoderms in oolitic layers.	Shallow marine, restricted.
MF-4 Bioclastic packstone	Poorly sorted packstone. Molluscan dominated, and few fine-grained ooids and peloids. Thin-shelled bivalves with bladed spar cement, some infilling mud and calcite spar within molluscan shells.	Abundant bivalves, including articulate, disarticulate and fragmented. Shells thin and long, some reach up to 10 mm in length. Minor small gastropods.	Shallow marine, low to medium energy.
MF-5 Bioclastic wackestone	Mud abundant, with minor amounts of bioclasts, peloids and ooids fragments.	–	Shallow subtidal, low energy.

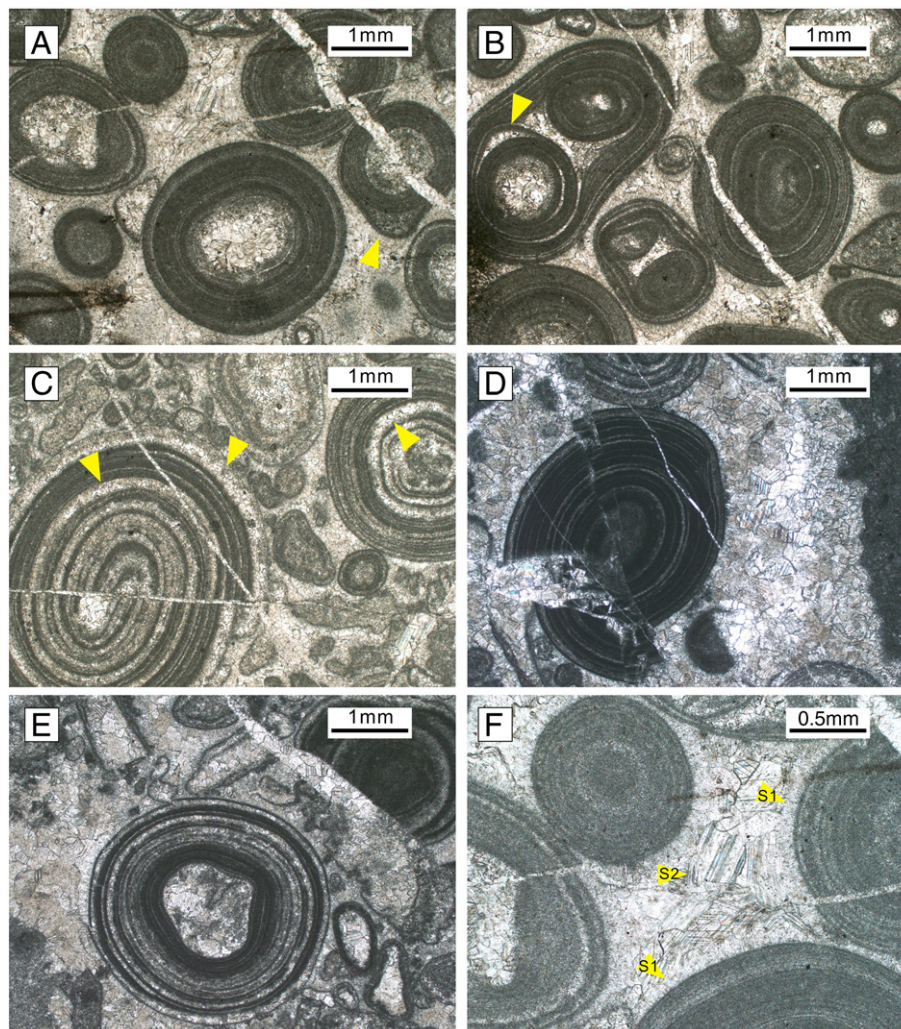


**Fig. 6.** Photomicrographs of giant ooids at Moyang section, plane-polarized light. (A) Giant ooids displaying concentric laminae, recrystallized (calcite-spar) nuclei, and well-preserved cements. Note the “domed ooid” (arrow). (B) Compound ooids composed of smaller ooids; note presence of “domed ooid” (arrow) in interior of compound ooid. (C) Giant ooids with selectively recrystallized laminae (arrow); note that recrystallized laminae tend to be thicker than well-preserved laminae. (D) Giant ooid comprise a succession of dense laminae. (E) The nucleus of giant ooid is composed of granular calcite grains which shape probably indicates its bioclastic origin. (F) Cements of giant ooids deposits. The first generation cements (S1) formed thin isopachous fringes (encircle ooids), and the second generation cements (S2) filled the remaining space. (For interpretation of the references to color in this figure legend, the reader is referred to the web version of this article.)

## 5. Discussion

### 5.1. Original mineralogy of ooid cortices

Like most ancient ooids, the Moyang giant ooids now consist entirely of low-Mg calcite, which show a pattern of thinly laminated cortical layers that is commonly associated with (although not strictly diagnostic of) a primary aragonitic mineralogy (Tucker, 1985; Flügel, 2004). Data compilations of the mineralogies of inorganic carbonate precipitates previously indicated that the Permian and Triassic periods had “aragonite seas” (c.f. Sandberg, 1983; Wilkinson et al., 1985). However, several lines of evidence suggest that the original mineralogies of these ooids need to be reconsidered. Interpretation of the original mineralogy of ooid cortices requires assessment of (1) morphology and orientation of crystallites in ooid cortical layers, (2) manner of preservation of ooid cortical layers, and (3) geochemical concentration data, especially of Sr. First, the cortical laminae of the Moyang ooids show contrasting preservation styles (Fig. 6), with the light-colored laminae exhibiting a coarsely sparry microstructure and the dark-colored laminae exhibiting preservation of fine microtextural detail that shows evidence of plentiful microbial activity (such as filamentous networks and biofilms; Fig. 6C and E).

The alternating styles of laminar preservation may be due to variation either in organic content or in original mineralogical composition (i.e., aragonite versus calcite). Third, the low Sr concentrations of the Moyang giant ooids (<1250 ppm) are indicative of a calcitic primary composition (e.g., modern inorganic calcite averages 1500–2000 ppm Sr; Kinsman, 1969) or mixed aragonitic–calcitic composition. A purely aragonitic primary mineralogy is unlikely because modern inorganic aragonite averages 8000–10,000 ppm Sr (Kinsman, 1969; Brand and Veizer, 1983; Duguid et al., 2010). Although the Sr concentrations of primary aragonite grains can decrease considerably as a consequence of recrystallization in an open diagenetic system, commonly at least some grains will preserve high Sr concentrations (Algeo and Watson, 1995). The Moyang ooids underwent recrystallization in a nearly closed diagenetic system, which should have preserved high Sr concentrations if the cortices had originally consisted of aragonite. In view of the petrographic characteristics and the low and relatively uniform Sr concentrations of the ooids, we infer the primary mineralogy of the Moyang ooids to have been either low-Mg calcite or a bimineralic composition (i.e., mixed aragonite–calcite) in which calcite probably predominated.

If Moyang ooid cortices bimineralic (which is possible, but not certain), it would have important implications for interpreting local and temporary variations in seawater chemistry. The observations of the

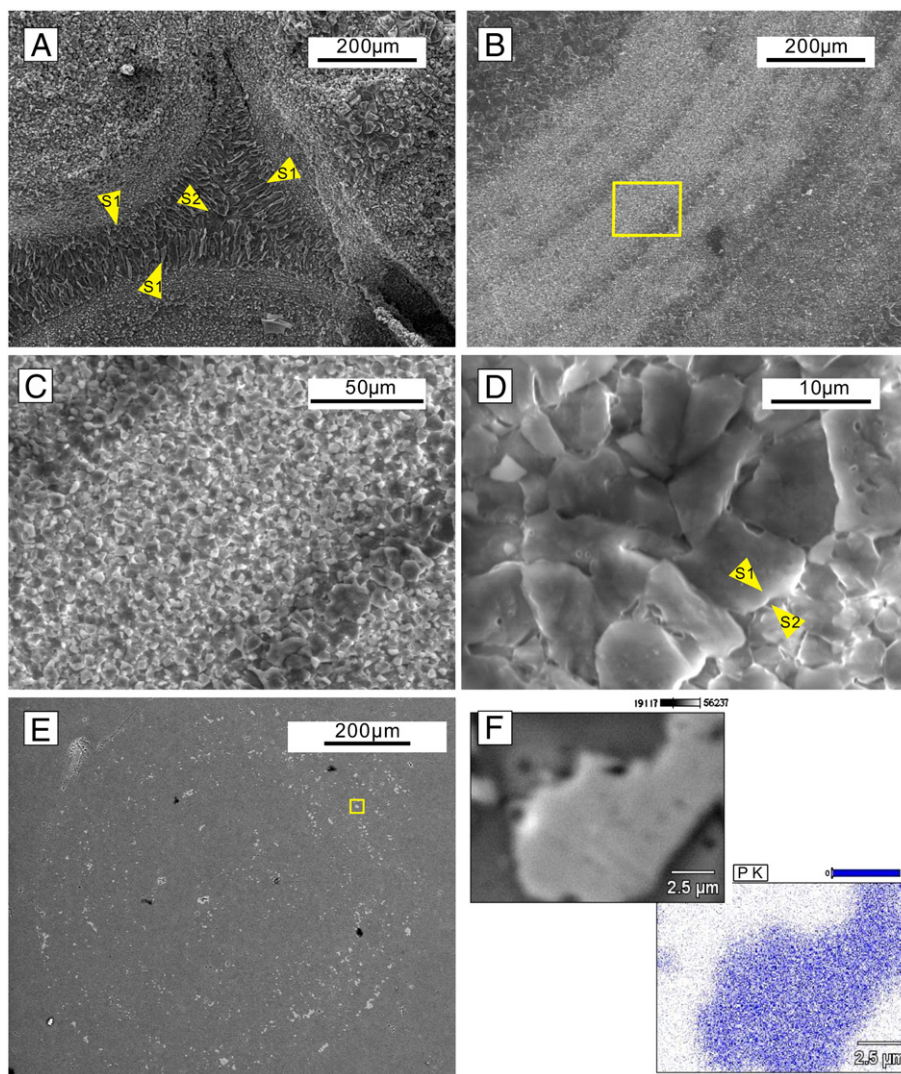


**Fig. 7.** Microstructural features present in giant-oid cortices. (A) SEM photomicrograph showing bladed (S1) and blocky (S2) cement between ooids. (B) Finely (bright) and coarsely (dark) crystalline laminae with distinct boundary. (C) Enlargement of the squared area in (B), note size variation of calcite-crystal across laminae. (D) High magnification view of the laminae. Coarse calcite crystals (S1) and fine calcite crystals (S2) are shown, respectively. (E) Polished slab of giant ooid under the SEM. Note granular minerals scattered concentrically in ooid cortices. (F) Detail of the mineral in (E), with content map of phosphorus under EPMA. (For interpretation of the references to color in this figure legend, the reader is referred to the web version of this article.)

present study suggest that Early Triassic seas were, in fact, poised between calcite and aragonite precipitation, and that small changes in carbonate equilibria may have caused frequent variation in precipitate mineralogy. This pattern had previously been observed in Upper Pennsylvanian ooids from southern Kansas (Wilkinson et al., 1984; Algeo

and Watson, 1995), where upwelling of anoxic deepwaters onto shallow carbonate shelves of the Midcontinent Sea (Algeo and Heckel, 2008) may have caused frequent fluctuations in carbonate saturation levels. In the case of Early Triassic oceans, previous studies have found extensive evidence of upwelling of anoxic deepwaters into shallow-

**Table 4**

Electron probe microanalysis results of giant-ooids samples from Moyang section.

	1#	2#	3#	4#	5#	6#	7#	8#	9#	10#	11#	12#	13#	14#	15#	Average <sup>a</sup>	Sigma
Na <sub>2</sub> O	0.030	0.148	0.047	0.014	0.030	0.098	–	0.041	0.022	0.052	0.005	0.055	0.003	0.008	–	0.037	0.041
CaO	56.577	56.621	55.366	54.161	55.497	55.392	55.783	55.595	55.648	55.345	55.633	55.519	55.373	55.314	55.337	55.544	0.563
CO <sub>2</sub>	42.910	*	43.538	45.277	43.722	44.099	41.512	41.375	43.100	43.163	43.569	42.938	43.578	43.858	43.329	40.398	11.216
MnO	0.015	–	–	0.063	0.029	–	0.094	0.010	0.026	–	–	–	–	0.026	0.029	0.019	0.027
MgO	0.102	0.030	0.233	0.301	0.297	0.201	0.375	0.225	0.253	0.309	0.073	0.318	0.110	0.171	0.160	0.211	0.101
P <sub>2</sub> O <sub>5</sub>	0.036	41.659	0.048	0.036	0.006	0.024	–	0.054	–	–	0.024	0.066	0.042	–	0.030	2.802	10.750
FeO	0.043	0.046	0.099	0.019	0.002	0.021	–	0.024	0.041	0.041	0.090	0.022	0.054	0.043	0.001	0.036	0.029
SiO <sub>2</sub>	0.045	0.061	0.069	0.063	0.079	0.070	0.066	0.052	0.034	0.043	0.038	0.051	0.094	0.049	0.023	0.056	0.018
SO <sub>3</sub>	–	0.419	0.018	0.010	–	0.028	0.038	–	0.034	–	–	0.030	–	–	0.012	0.039	0.106
SrO	0.099	0.146	0.146	0.085	0.066	0.091	0.128	0.040	0.133	0.067	0.108	0.092	0.087	0.080	0.079	0.096	0.031

Note: “–” means value below detection limit, and “\*\*” means influenced by coating carbon film. Unit: wt.%.

<sup>a</sup> The average value of each element used in text excluding sample 2# (phosphate mineral).

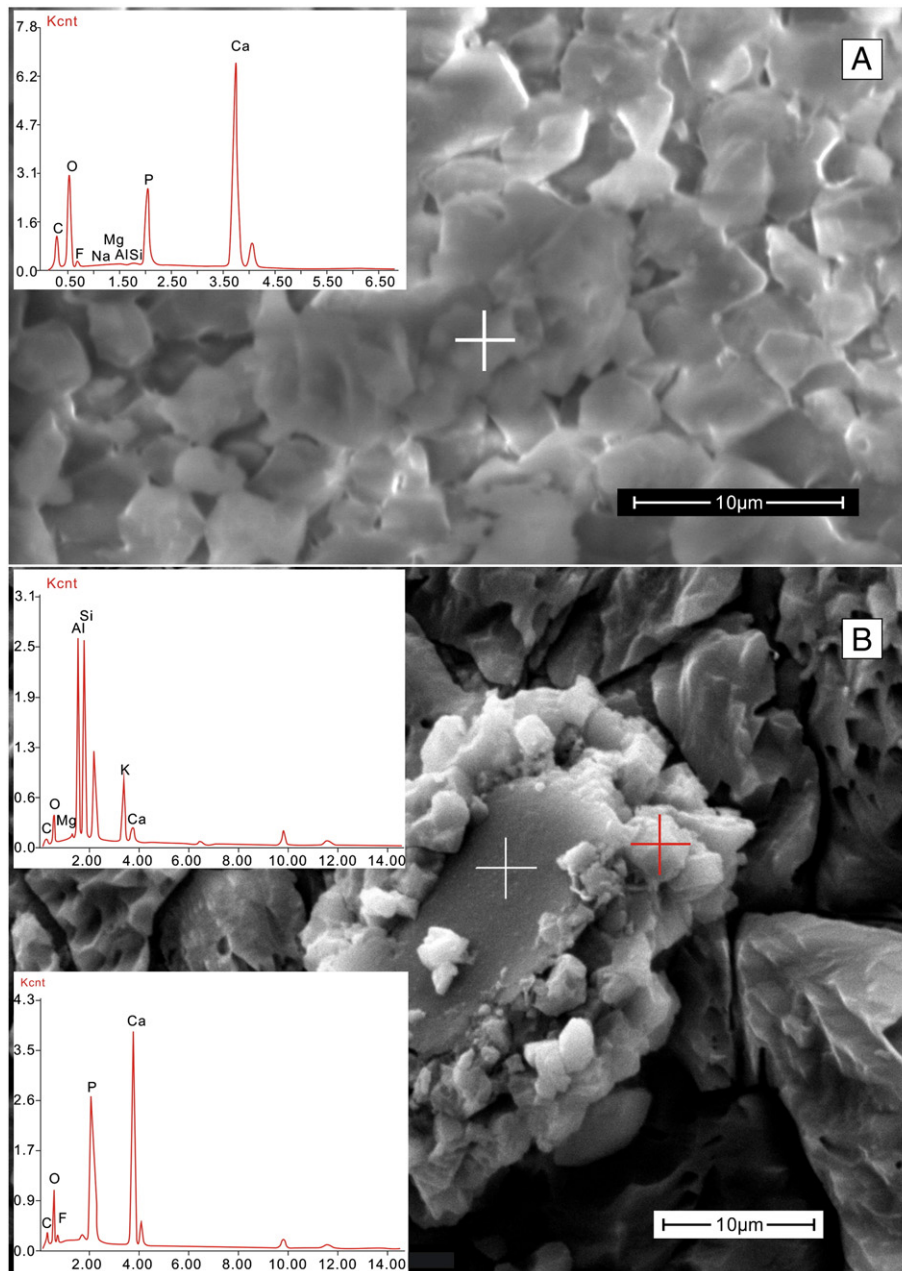


**Fig. 8.** SEM photomicrographs combined with EDS analysis for phosphate mineral. (A) An assemblage with tube-like structure in finely crystalline laminae. It is consisted of a P-rich and F-bearing mineral on EDS result. (B) Granular phosphate minerals (red cross; correspond to the lower left inserted curve) accumulate out of illite-like mineral with high Al, Si and K (white cross; correspond to the upper left inserted curve). (For interpretation of the references to color in this figure legend, the reader is referred to the web version of this article.)

marine systems (e.g. Grice et al., 2005; Algeo et al., 2007). Upwelling events mix undersaturated deepwaters with supersaturated surface waters, leading to rapid changes in carbonate equilibria and saturation state that may be recorded as ooid laminae of alternating mineralogies. Since such processes can be markedly local in their scale of operation, determining whether the Early Triassic global ocean was truly an “aragonite sea” will require more data from a broader range of locales.

### 5.2. Formation of CFA in ooid cortices

Carbonate fluorapatite (CFA) is the dominant phosphate mineral occurring in early diagenetic marine environments (Ruttenberg and Berner, 1993; Föllmi, 1996; Compton et al., 2000). It forms not only in upwelling-associated phosphorite environments (e.g., Glenn and Arthur, 1988) but also in non-upwelling environments such as paralic and deltaic facies dominated by siliciclastic sediments, as well as on

continental margins with low sedimentation rates (e.g., Baturin, 1988; Heggie et al., 1990; O'Brien et al., 1990; Ruttenberg and Berner, 1993). The two most important processes influencing CFA precipitation are (1) organic matter degradation and release of biogenic phosphate to porewater (Krajewski et al., 1994; Konhauser, 2007; Arning et al., 2009), and (2) redox cycling of Fe, which enriches inorganic phosphate in the sediment by absorption onto Fe-(oxyhydr)oxides (Heggie et al., 1990; Nelson et al., 2010). The formation of CFA and associated microbial activity can be widely traced in the ancient phosphogenic record, and research on both stromatolitic phosphorite and coated phosphate grains provide examples of these processes (Soudry and Southgate, 1989; Gächter and Meyer, 1993; Krajewski et al., 1994; Krajewski et al., 2000; Soudry, 2000).

Precipitation of CFA within ooid cortices is considered to indicate a microbially mediated process (Horton et al., 1980; Dahanayake and Krumbein, 1985; Glenn and Arthur, 1988; Pufahl and Grimm, 2003).

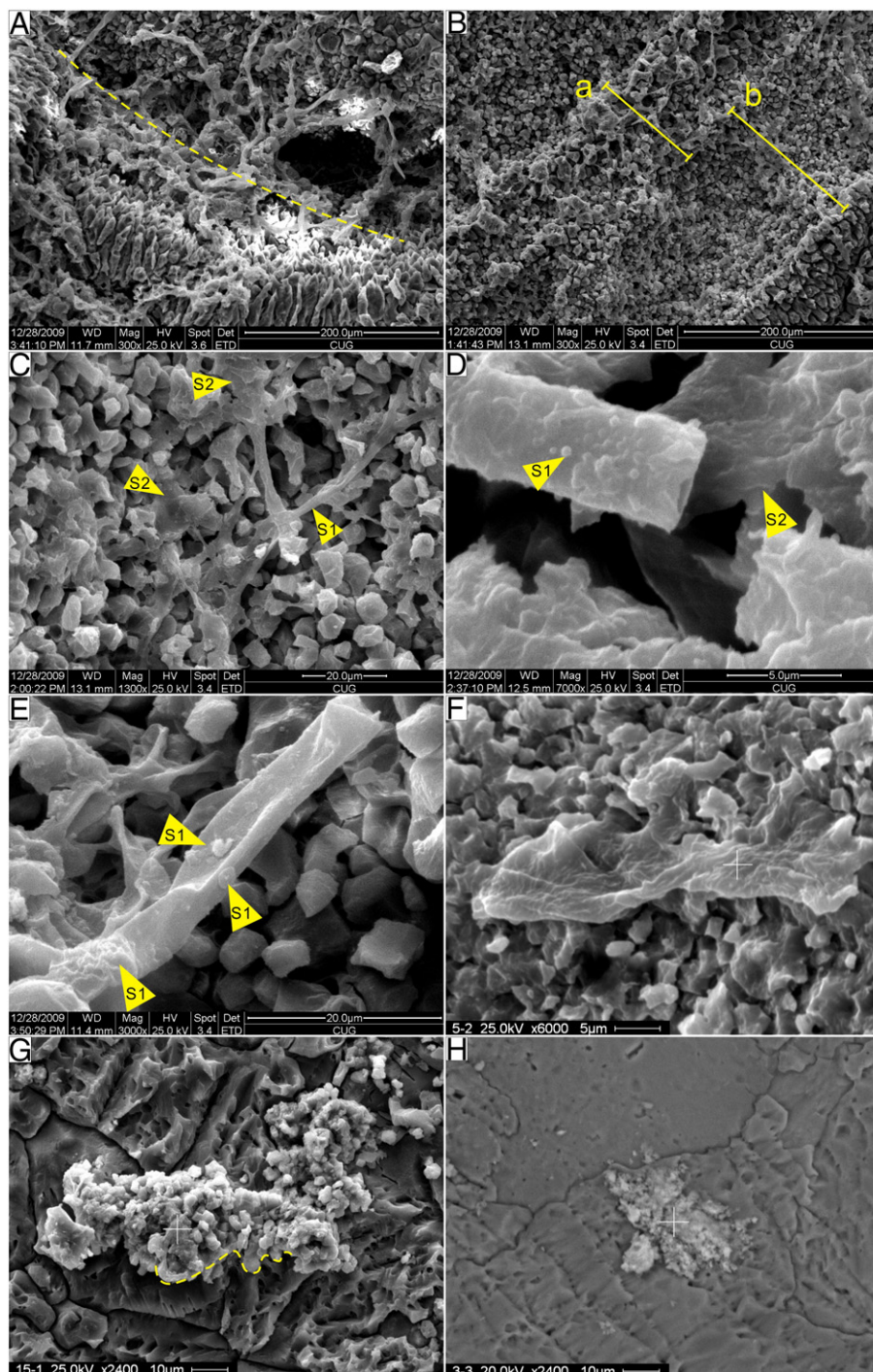


**Fig. 9.** SEM photomicrographs highlighting microbial fabric and authigenic mineral in giant-oid cortices. (A) Microborings in ooid cortices. Note the growth direction of microborings is roughly perpendicular to contact surface (the dotted line is the boundary between ooid and matrix). (B) Giant-oid laminae after etching treatment. Note (a) is coarsely crystalline lamina, and (b) is finely crystalline lamina. (C) Magnified image of part (b). Note abundant filamentous microbes (S1) occupy intercrystalline space and mucilaginous films (S2) drape over calcite crystals. (D) Close-up view of microbes. The filament is 5.0  $\mu\text{m}$  in diameter, hollow tube, with cocoid-like globules (S1) on its surface. The fabric of mucilaginous films (S2) covers calcite crystals. (E) Depressed microbial tube with some tiny calcite crystals (S1) on its surface. (F) Organic remains of films with a high content of carbon. (G) Granular phosphate minerals covering a film-like fabric (the dotted line is the boundary). (H) Ferric oxides in ooid cortices.

Ooid growth can occur through both inorganic carbonate precipitation and microbial calcification (e.g., biofilms and/or microborings), although the extent to which the latter process influences ooid generation remains controversial (Simone, 1981; Gerdes et al., 1994; Duguid et al., 2010). Microbes dwelling on ooid surfaces actively absorb and store dissolved phosphate (Gächter et al., 1988; Gächter and Meyer, 1993). In addition, microbial biofilms on the surfaces of ooids may behave as physical barriers reducing the diffusion of

phosphate back into the water column (Konhauser, 2007), and precipitation of additional laminae encloses phosphate within the ooid cortex. Where conditions are favorable, a large quantity of phosphate can be preserved in ooid cortices. Upon death of the microbes, phosphate is released into the closed cortical porewater environment via heterotrophic degradation (Gulbrandsen, 1969; Konhauser, 2007), a process that creates local sites of supersaturation with respect to CFA and leads to its precipitation along specific laminar surfaces

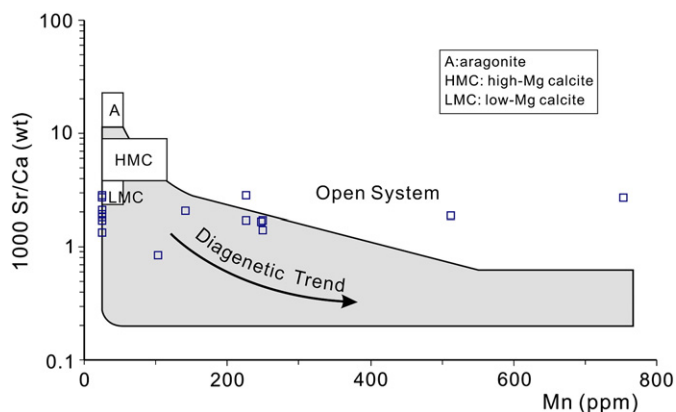


**Fig. 10.** Diagram of diagenetic chemical trend for coated grains (base map from Brand and Veizer, 1980, 1983). Manganese values at the far left correspond to data of giant ooids that below EPMA detection limit.

(Van Cappellen and Berner, 1991; Krajewski et al., 1994). In the giant ooids of Moyang, such surfaces are mainly finely crystalline laminae that contain illite and the remains of microbial biofilms (e.g., Fig. 7).

One hypothesis to account for the precipitation of CFA in Early Triassic giant ooids is introduction of dissolved organic phosphorus (DOP) through incursion of anoxic watermasses of deep-marine origin into shallow-marine settings (“deepwater P source” model; Fig. 12A). During the latest Permian, ocean anoxia was widespread in deep-water environments (Kajiwara et al., 1994; Wignall and Twitchett, 1996; Isozaki, 1997; Grasby and Beauchamp, 2009; Algeo et al., 2010). These deep waters were rich in  $\text{CO}_2$ , DOP, and  $\text{H}_2\text{S}$  and poor in dissolved oxygen (Knoll et al., 1996) owing to aerobic and anaerobic decay of organic matter. Transfer of watermasses with such chemistry into shallow-marine settings might have occurred through either episodic chemocline upward excursion (Kump et al., 2005) or upwelling events (Algeo et al., 2007). Regardless of the exact mechanism, incursions of anoxic deep watermasses into shallow-marine environments seem to have occurred episodically during the Early Triassic (Algeo et al., 2007; Korte and Kozur, 2010). Incursions of phosphate-rich deep waters into shallow-marine environments would have caused changes in water chemistry that influenced the formation of ooids.

A second hypothesis to account for the precipitation of CFA in Early Triassic giant ooids invokes concentration of phosphate at the sediment–water interface through adsorption onto ferric (oxyhydr)oxides (“sediment P source” model; Fig. 12B). Ferric (oxyhydr)oxides serve to trap dissolved phosphate released from decaying organic

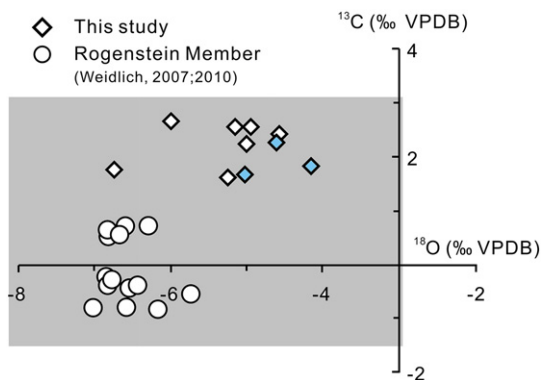


**Fig. 11.** Plots of  $\delta^{13}\text{C}$  and  $\delta^{18}\text{O}$  data of giant-ooids from Moyang, contrast with those of the Rogenstein Member of Germany (Weidlich, 2007, 2010). The shaded region is the major interval of a series of published data of the Early Triassic (Baud et al., 1989; Veizer et al., 1999; Payne et al., 2004; Korte et al., 2005; Korte and Kozur, 2010). Note matrix samples are colored. (For interpretation of the references to color in this figure legend, the reader is referred to the web version of this article.)

matter and prevent its release into the overlying water column (Föllmi, 1996; Algeo and Ingall, 2007). In settings in which the redox ( $\text{O}_2$ – $\text{H}_2\text{S}$ ) interface is located at or close to the sediment–water interface, this process can make phosphate available for transfer onto ooid growth surfaces (Heggie et al., 1990). Fluoride, another component of CFA, may also adsorb onto ferric (oxyhydr)oxide surfaces in marine sediments (Ruttenberg and Berner, 1993). When ooids are in either the rolling or stationary stage, microbes living on ooid surfaces are able to bind these ferric (oxyhydr)oxides and capture them from the sediment–water interface. After enclosure within the ooid cortex through precipitation of additional laminae, organic carbon oxidation reactions cause reduction of ferric iron to ferrous iron and release of adsorbed phosphate into the closed cortical pore-water environment. Dissolved phosphate trapped in this manner is ultimately precipitated as CFA along specific ooid laminar surfaces that are also enriched in sedimentary iron (Fig. 9H). One major requirement of this hypothesis is that sufficient organic carbon (presumably of microbial origin) be present within the ooid cortex to drive reductive release of phosphate and ferric (oxyhydr)oxides.

### 5.3. Formation of giant ooids in the Early Triassic

The main controls on the generation of giant ooids are thought to be reduced nucleus supply, increased growth rate, and higher environmental energy levels (Sumner and Grotzinger, 1993). A reduced supply of nuclei means low skeletal grain abundance that may, if possible, influence both regional carbonate saturation state and local carbonate removal mechanisms due to the absence of a dominant skeletal sink of calcium carbonate (Payne et al., 2006a). Carbonate saturation state has a great influence on cortical growth rate (Swett and Knoll, 1989; Opdyke and Wilkinson, 1993; Sumner and Grotzinger, 1993), so highly supersaturated conditions favor faster growth rates and larger ooids generally. Environmental energy levels are commonly a function of facies patterns. Carbonate ramps possess unprotected margins that allow waves and currents to penetrate easily into ramp interiors, thus creating more agitated conditions in shallow-water facies (Sumner and Grotzinger, 1993). Episodic hydrodynamic events such as associated with storms may play an important role in giant ooid formation. Mobilization and growth of ooids can occur only when the energy threshold needed to put in motion an ooid of a given size is exceeded, and larger ooids will have larger energy thresholds (Heller et al., 1980). Even large ooids that are buried in shallow sediments most of the time can be remobilized and have additional cortical layers added if energy levels are sufficiently high. Ooid growth can continue through this process as long as the mass gained during remobilization events is greater than the mass lost through abrasion.

Several factors favoring formation of giant ooids may have existed following the end-Permian mass extinction. First, the absence of a dominant skeletal sink of  $\text{CaCO}_3$  caused by marine mass extinction and subsequent incursions of sulfidic deepwaters that may have episodically “sterilized” shallow-marine shelves (Algeo et al., 2007; Korte and Kozur, 2010) would be more likely to elevate the level of  $\text{CaCO}_3$  saturation in seawater and cause carbonate deposition to switch to microbially- and/or abiotically-induced forms of precipitation (Payne et al., 2006a). Second, such incursions of deepwaters rich in  $\text{HCO}_3^-$ ,  $\text{CO}_2$  and  $\text{H}_2\text{S}$  (Kajiwara et al., 1994; Grotzinger and Knoll, 1995; Knoll et al., 1996; Kump et al., 2005) created chemical conditions that, at least locally, resulted in massive precipitation of inorganic carbonates in shallow-marine settings. High  $\text{HCO}_3^-$  concentrations serve to increase both  $\Sigma \text{CO}_2$  and alkalinity and, hence, the saturation state of a watermass with respect to  $\text{CaCO}_3$  (Kempe, 1990), and the global decline of skeletal organisms in this interval may have helped to sustain such conditions. Third, geographic factors may have played a role. The enormous carbonate ramp that adjoined the Yangtze Platform during the Early Triassic (Fig. 1B) allowed

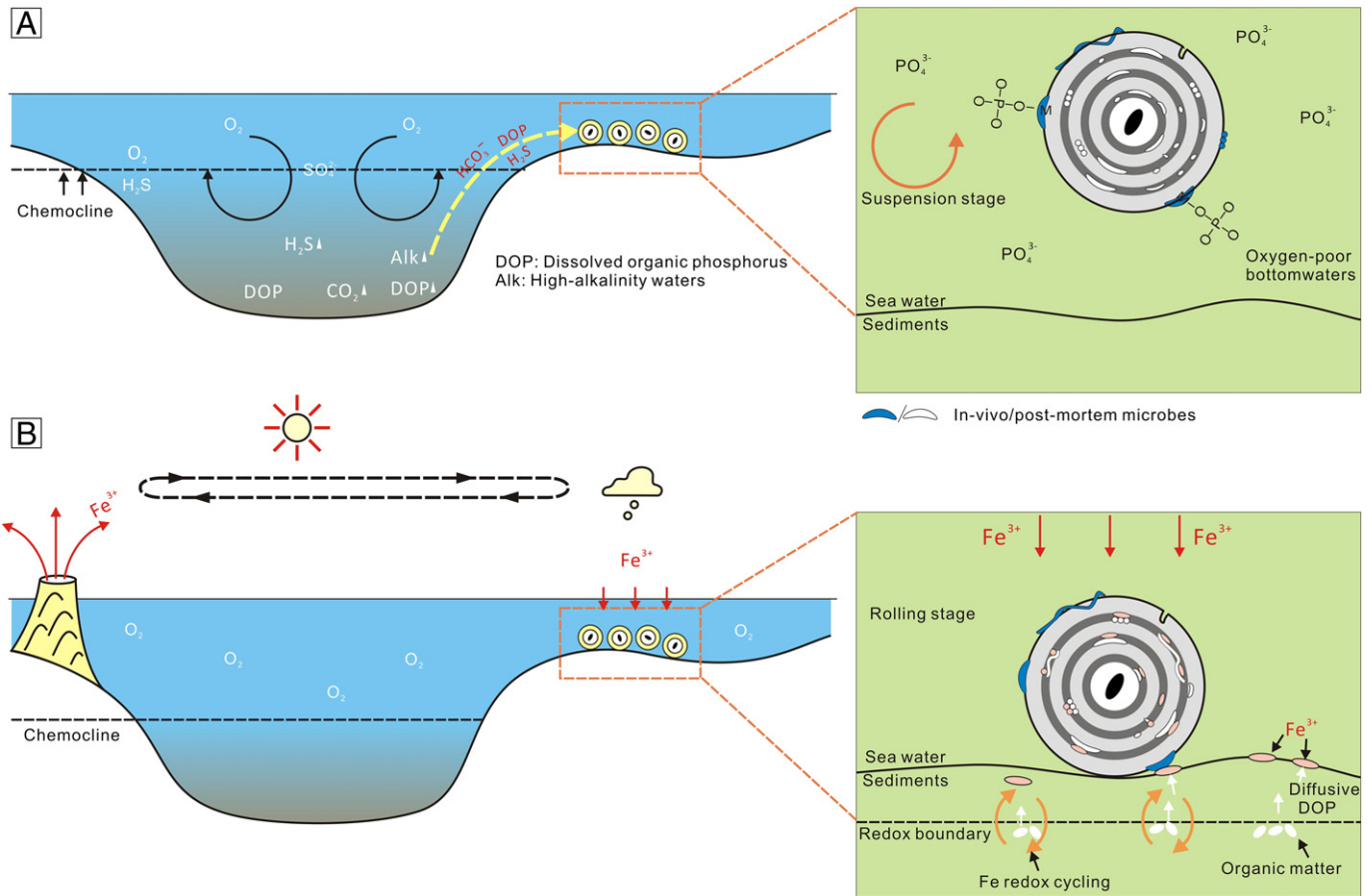


**Fig. 12.** Two hypotheses proposed for the generation of CFA in ooid cortex. (A) “Deepwater P source” model. Decay of organic matter yields deep waters rich in CO<sub>2</sub>, DOP, and H<sub>2</sub>S, which are introduced into the shallow-marine environment at Moyang through episodic chemocline upward excursion and/or upwelling events. (B) “Sediment P source” model. Dissolved phosphate released from decaying organic matter at the sediment–water interface is initially trapped by ferric (oxyhydr)oxides, subsequently bound onto ooid surfaces by microbes, and finally desorbed via organic carbon oxidation reactions. See Section 5.2 for further details.

frequent storms and currents to transfer energy into ramp interiors, promoting giant ooid formation.

The chemical conditions most favorable for giant ooid formation appear to have been associated with times of increasing carbonate

$\delta^{13}\text{C}$  values and more widespread ocean anoxia (Fig. 2B). The association between the latter features was probably due to development of Early Triassic ocean anoxia primarily as a result of elevated levels of marine primary productivity (Algeo et al., 2011), which served to

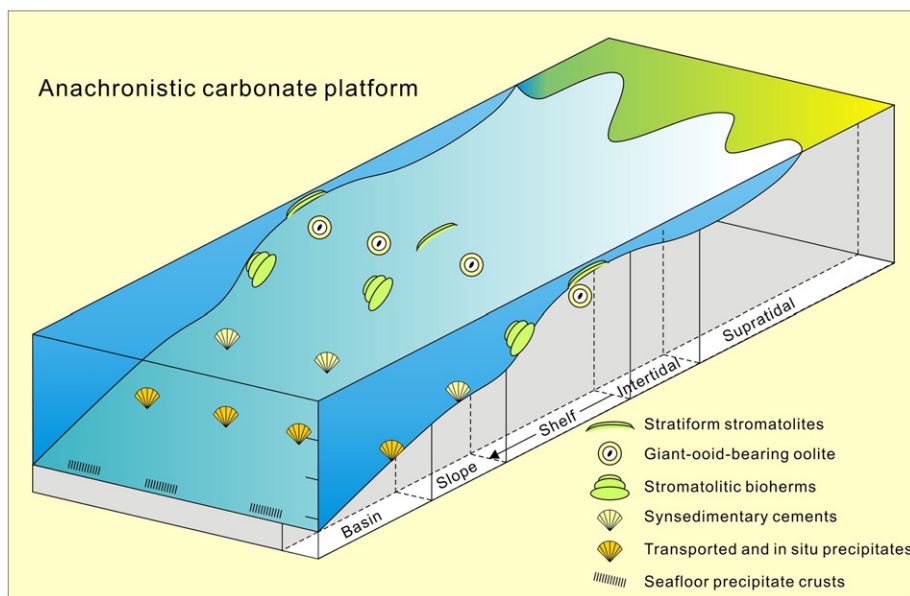


**Fig. 13.** Model of anachronistic carbonate platform (modified from Woods et al., 2007) shows the distribution of a series of anachronistic facies from basin to shallow water. The origin of these special sediments relates to carbonate supersaturation state which probably induced by alkaline deep-waters mixing with shallow waters, or progressively reaching shelf depositional settings.

drive expansion of anoxia in oceanic oxygen–minimum zones (Algeo et al., 2010) and to simultaneously deplete dissolved inorganic carbon of the light isotope of carbon ( $^{12}\text{C}$ ) in seawater. Giant ooids formed in conjunction with episodes of elevated marine productivity because of the resulting increased levels of alkalinity and carbonate saturation in seawater. These episodes were concentrated in the early Griesbachian, the Dienerian, and the late Smithian (Fig. 2B; Payne et al., 2004; Galfetti et al., 2007). Thus, the Early Triassic was a time period that was especially suitable for the generation of giant ooids.

#### 5.4. Giant ooids as an anachronistic facies

Tabulation of the occurrences of giant ooids through Earth history (Table 1) illustrates that most marine carbonate giant ooids are found in Precambrian sediments (Flügel, 1982; Richter, 1983; Sumner and Grotzinger, 1993; Trower and Grotzinger, 2010). They have been rare through the Phanerozoic, seemingly only generated during specific episodes of Late Cambrian, Early Triassic, and Middle–Late Jurassic age. As shown in this study, giant ooids were generated widely in tropical shallow-marine settings during the Early Triassic, but by the Middle Triassic only normal-sized (<2 mm) ooids are found in oolitic facies.

During the Early Triassic, giant ooids were not a local phenomenon but, rather, widely developed across the eastern Tethyan region. Before this study, the oldest confirmed giant-ooid deposit is located in the Griesbachian substage of the Cili section (Hunan Province) (personal observation, 2008 and Wang et al., 2009), but that occurrence is younger than the Moyang giant ooids, which are of latest Permian age (Fig. 4C and D). Giant ooids of approximately the same age with Moyang have also been reported from the Germanic Basin in the western Tethyan region (Fig. 1A-1; Weidlich, 2007). In China, many giant ooid deposits are found in the Dienerian and earliest Smithian substages (Fig. 2), including on the southern (Fig. 1B-5; Wang et al., 2005) and northern margins (Fig. 1B-6; X. Tan, personal communication, 2010) of the Upper Yangtze Platform, on the northern Middle Yangtze Platform (Fig. 1B-7; Daye area, Hubei Province), and on the Lower Yangtze Platform (Songsan section of Wuxi, Jiangsu Province) (Fig. 1B-8; Y. Wang, personal communication, 2010), as well as on isolated carbonate platforms in the Nanpanjiang Basin (Fig. 1B-4; Guangxi Bureau of Geology Mineral Resources, 1972; Payne et al., 2006b; Lehrmann et al., 2007). Some younger occurrences of giant ooids have been reported from the middle–late Olenekian of the Lower Yangtze Platform (Feng et al., 1988), the Shuanghu area of the Qiangtang Block (northern Tibet) (Fig. 1A-2; Zhu et al., 2005), and the Yidun Block in southwestern China (Fig. 1A-3; Hou et al., 1991).

The depth of formation of giant ooids was generally shallow, probably within the intertidal to upper subtidal range, making them some of the shallower features of the “anachronistic carbonate platform” model (Fig. 13; Pruss et al., 2005; Woods et al., 2007; Mary and Woods, 2008). Thus, a series of unusual sediments or structures from basinal to intertidal settings constituted the anachronistic depositional system of the Early Triassic. In South China, giant-ooid-bearing oolitic facies are usually found in association with microbialites (Qian and Fan, 1994; Wang et al., 2009) and flat-pebble conglomerates. The spatial and temporal distribution of giant ooid facies of Early Triassic age mirrors that of other anachronistic deposits such as microbialites because development of all of these facies was favored by the increased carbonate saturation levels induced by incursion of highly alkaline deep waters into shallow-water environments.

## 6. Conclusions

Giant ooids are a type of anachronistic facies that resulted from perturbed oceanic conditions following the end-Permian crisis. They are associated with other anachronistic facies (such as microbialites and seafloor carbonate cement fans) that were favored also by the

episodic incursion of alkaline deep waters into shallow-marine environments. Giant ooids in the study section at Moyang (South China) have cortices that are finely laminated, show generally good preservation, and have trace-element and isotopic compositions consistent with limited diagenesis in a relatively closed system. These microstructural features facilitated preservation of CFA, concentrations of which along the laminar surfaces of Moyang giant ooids provide new insights into paleoceanographic conditions during the Early Triassic. Episodic incursions of deep waters onto shallow-marine ramps of the Yangtze Platform stimulated giant ooid production through increased watermass agitation and carbonate saturation levels as well as reduced carbonate removal rates through biotic skeletal formation. The high phosphate content of these deep waters allowed enhanced absorption of P onto ooid surfaces by microbial activity, with subsequent diagenetic conversion to CFA microcrystals. Microfacies analysis shows that the environmental conditions favoring giant ooid formation were inimical to metazoans, and that giant ooids disappeared as benthic marine communities recovered during the Early Triassic. This study offers a new perspective on the controls on giant ooid formation and their relationship to disaster periods in Earth history.

## Acknowledgments

The study presented in this paper comes from work carried out by F. Li at the China University of Geosciences for a M.S. degree. We thank Dr. S. Zhang for her help during SEM examination, Dr. S. Zheng for assistance in EPMA analysis, and Dr. Y. Sun who helped with conodont samples. We also thank Y. Wang and X. Tan for helpful discussions, X. Wang, B. Li and J. Cao for their assistance in the field. We greatly appreciate Sierd Cloetingh for editorial handling, and two anonymous reviewers for their valuable comments. This research was supported by National Natural Science Foundation of China (grant no. 41072078) and the “111 project” of Chinese State Administration of Foreign Experts Affairs (grant no. B08030). This study is a contribution to IGCP Project 572.

## References

- Algeo, T.J., Heckel, P.H., 2008. The Late Pennsylvanian midcontinent sea of North America: a review. *Palaeogeography Palaeoclimatology Palaeoecology* 268 (3–4), 205–221.
- Algeo, T.J., Ingall, E., 2007. Sedimentary  $\text{C}_{\text{org}}:\text{P}$  ratios, paleocean ventilation, and Phanerozoic atmospheric  $\text{pO}_2$ . *Palaeogeography Palaeoclimatology Palaeoecology* 256 (3–4), 130–155.
- Algeo, T.J., Watson, B.A., 1995. Calcite, aragonite, and bimineralic ooids in Missourian (Upper Pennsylvanian) strata of Kansas: stratigraphic and geographic patterns of variation. In: Pausé, P.H., Candelaria, M.P. (Eds.), *Carbonate Facies and Sequence Stratigraphy: Practical Applications of Carbonate Models: Permian Basin Section*. SEPM, Publ. 95–36, pp. 141–173.
- Algeo, T.J., Ellwood, B., Nguyen, T.K.T., Rowe, H., Maynard, J.B., 2007. The Permian–Triassic boundary at Nhi Tao, Vietnam: evidence for recurrent influx of sulfidic watermasses to a shallow-marine carbonate platform. *Palaeogeography Palaeoclimatology Palaeoecology* 252 (1–2), 304–327.
- Algeo, T.J., Hinnov, L., Moser, J., Maynard, J.B., Elswick, E., Kuwahara, K., Sano, H., 2010. Changes in productivity and redox conditions in the Panthalassic Ocean during the latest Permian. *Geology* 38 (2), 187–190.
- Algeo, T.J., Chen, Z.Q., Fraiser, M.L., Twitchett, R.J., 2011. Terrestrial-marine teleconnections in the collapse and rebuilding of Early Triassic marine ecosystems. *Palaeogeography Palaeoclimatology Palaeoecology*. doi:10.1016/j.palaeo.2011.01.011.
- Amsden, T.W., Barrick, J.E., 1986. Late Ordovician–Early Silurian strata in the central United States and the Hirnantian Stage. *Bulletin of Oklahoma Geological Survey* 139, 1–95.
- Arning, E.T., Birgel, D., Brunner, B., Peckmann, J., 2009. Bacterial formation of phosphatic laminites off Peru. *Geobiology* 7 (3), 295–307.
- Bates, N.R., Brand, U., 1990. Secular variation of calcium carbonate mineralogy: an evaluation of ooid and micrite chemistries. *Geologische Rundschau* 79 (1), 27–46.
- Batten, K.L., Narbonne, G.M., James, N.P., 2004. Paleoenvironments and growth of early Neoproterozoic calcimicrobial reefs: platform Little Dal Group, northwestern Canada. *Precambrian Research* 133 (3–4), 249–269.
- Baturin, G.N., 1988. Disseminated phosphorus in oceanic sediments: a review. *Marine Geology* 84 (1–2), 95–104.
- Baud, A., Magaritz, M., Holser, W.T., 1989. Permian–Triassic of the Tethys: carbon isotope studies. *Geologische Rundschau* 78 (2), 649–677.

- Baud, A., Cirilli, S., Marcoux, J., 1997. Biotic response to mass extinction: the lowermost Triassic microbialites. *Facies* 36, 238–242.
- Baud, A., Richoz, S., Pruss, S., 2007. The lower Triassic anachronistic carbonate facies in space and time. *Global and Planetary Change* 55 (1–3), 81–89.
- Beukes, N.J., 1983. Ooids and oolites of the proterophytic Boomplaas Formation, Transvaal Supergroup, Griqualand West, South Africa. In: Peryt, T.M. (Ed.), *Coated Grains*. Springer-Verlag, Berlin, pp. 199–214.
- Bosellini, A., Masetti, D., Sarti, M., 1981. A Jurassic “Tongue of the Ocean” infilled with oolitic sands: the Belluno Trough, Venetian Alps, Italy. *Marine Geology* 44 (1–2), 59–95.
- Brand, U., Veizer, J., 1980. Chemical diagenesis of a multicomponent carbonate system-1: trace elements. *Journal of Sedimentary Research* 50 (4), 1219–1236.
- Brand, U., Veizer, J., 1981. Chemical diagenesis of a multicomponent carbonate system-2: stable isotopes. *Journal of Sedimentary Research* 51 (3), 0987–0997.
- Brand, U., Veizer, J., 1983. Origin of coated grains: trace element constraints. In: Peryt, T.M. (Ed.), *Coated Grains*. Springer-Verlag, Berlin, pp. 9–26.
- Chow, N., James, N.P., 1987. Facies-specific, calcitic and bimineralic ooids from Middle and Upper Cambrian platform carbonates, western Newfoundland, Canada. *Journal of Sedimentary Research* 57 (5), 907–921.
- Clough, J.G., Goldhammer, R.K., 2000. Evolution of the Neoproterozoic Katakaturuk Dolomite ramp complex, northeastern Brooks Range, Alaska. In: Grotzinger, J.P. (Ed.), *Carbonate Sedimentation and Diagenesis in the Evolving Precambrian World*. SEPM Spec. Publ., pp. 209–241.
- Collin, P.-Y., Kershaw, S., Crasquin-Soleau, S., Feng, Q., 2009. Facies changes and diagenetic processes across the Permian–Triassic boundary event horizon, Great Bank of Guizhou, South China: a controversy of erosion and dissolution. *Sedimentology* 56 (3), 677–693.
- Compton, J., Mallinson, D., Glenn, C.R., Filippelli, G., Föllmi, K., Shields, G., 2000. Variations in the global phosphorus cycle. In: Glenn, C.R. (Ed.), *Marine Authigenesis: From Global to Microbial*. SEPM Spec. Publ., pp. 21–33.
- Corsetti, F.A., Baud, A., Marengo, P.J., Richoz, S., 2005. Summary of Early Triassic carbon isotope records. *Comptes Rendus Palevol* 4 (6–7), 473–486.
- Corsetti, F.A., Kidder, D.L., Marengo, P.J., 2006. Trends in oolite dolomitization across the Neoproterozoic–Cambrian boundary: a case study from Death Valley, California. *Sedimentary Geology* 191 (3–4), 135–150.
- Dahanayake, K., Krumbein, W.E., 1985. Ultrastructure of a microbial mat-generated phosphorite. *Mineralium Deposita* 20 (4), 260–265.
- Davaud, E., Girardclos, S., 2001. Recent freshwater ooids and oncoids from western Lake Geneva (Switzerland): indications of a common organically mediated origin. *Journal of Sedimentary Research* 71 (3), 423–429.
- Day, E.S., James, N.P., Narbonne, G.M., Dalrymple, R.W., 2004. A sedimentary prelude to Marinoan glaciation, Cryogenian (middle Neoproterozoic) Keele Formation, Mackenzie Mountains, northwestern Canada. *Precambrian Research* 133 (3–4), 223–247.
- Duguid, S.M.A., Kyser, T.K., James, N.P., Rankey, E.C., 2010. Microbes and ooids. *Journal of Sedimentary Research* 80 (3), 236–251.
- Edzward, J.K., Toensing, D.C., Leung, M.C.-Y., 1976. Phosphate adsorption reactions with clay minerals. *Environmental Science and Technology* 10 (5), 485–490.
- Enos, P., 1995. Permian of China. In: Scholle, P.A., Peryt, T.M., Ulmer-Scholle, D.S. (Eds.), *The Permian of Northern Pangea*. Springer-Verlag, Berlin, pp. 225–256.
- Erwin, D.H., 1993. The Great Paleozoic Crisis: Life and Death in the Permian. Columbia University Press, New York, 327 pp.
- Erwin, D.H., 1994. The Permian–Triassic extinction. *Nature* 367 (6460), 231–236.
- Feng, Z., Wang, Y., Li, S., Xia, Y., 1988. Study on Lithofacies Paleogeography of Qinglong Group of Lower–Middle Triassic in the Lower Yangtze River Region. Yunnan Science and Technology Press, Kunming, 197 pp. (in Chinese with English abstract).
- Feng, Z., Bao, Z., Li, S., 1997. Lithofacies Paleogeography of Middle and Lower Triassic of South China. Petroleum Industry Press, Beijing, 222 pp. (in Chinese with English abstract).
- Flügel, E., 1982. *Microfacies Analysis of Limestones*. Springer-Verlag, Berlin, 633 pp.
- Flügel, E., 2004. *Microfacies of Carbonate Rocks: Analysis, Interpretation and Application*. Springer-Verlag, Berlin, 976 pp.
- Folk, R.L., 1993. SEM imaging of bacteria and nanobacteria in carbonate sediments and rocks. *Journal of Sedimentary Research* 63 (5), 990–999.
- Föllmi, K.B., 1996. The phosphorus cycle, phosphogenesis and marine phosphate-rich deposits. *Earth-Science Reviews* 40 (1–2), 55–124.
- Fraiser, M.L., Twitchett, R.J., Bottjer, D.J., 2005. Unique microgastropod biofacies in the Early Triassic: indicator of long-term biotic stress and the pattern of biotic recovery after the end-Permian mass extinction. *Comptes Rendus Palevol* 4 (6–7), 543–552.
- Frank, T.D., Wilkinson, B.H., Lohmann, K.C., 1993. Origin of submarine pisoliths and the sedimentology of midwestern Silurian reefs. *Journal of Sedimentary Research* 63 (6), 1070–1077.
- Gächter, R., Meyer, J.S., 1993. The role of microorganisms in mobilization and fixation of phosphorus in sediments. *Hydrobiologia* 253 (1), 103–121.
- Gächter, R., Meyer, J.S., Mares, A., 1988. Contribution of bacteria to release and fixation of phosphorus in lake sediments. *Limnology and Oceanography* 33 (6), 1542–1558.
- Gaetani, M., Angiolini, L., Ueno, K., Nicora, A., Stephenson, M.H., Sciunnach, D., Rettori, R., Price, G.D., Sabouri, J., 2009. Pennsylvanian–Early Triassic stratigraphy in the Alborz Mountains (Iran). In: Brunet, M.F., Wilmsen, M., Granath, J.W. (Eds.), *South Caspian to Central Iran Basins*. Geological Society of London Spec. Publ., London, pp. 79–128.
- Galfetti, T., Bucher, H., Ovtcharova, M., Schaltegger, U., Brayard, A., Brühwiler, T., Goudemand, N., Weissert, H., Hochuli, P.A., Cordey, F., Guodun, K., 2007. Timing of the Early Triassic carbon cycle perturbations inferred from new U–Pb ages and ammonoid biochronozones. *Earth and Planetary Science Letters* 258 (3–4), 593–604.
- Gerdes, G., Dunajtschik-Piewak, K., Riege, H., Taher, A.G., Krumbein, W.E., Reineck, H.E., 1994. Structural diversity of biogenic carbonate particles in microbial mats. *Sedimentology* 41 (6), 1273–1294.
- Glenn, C.R., Arthur, M.A., 1988. Petrology and major element geochemistry of Peru margin phosphorites and associated diagenetic minerals: authigenesis in modern organic-rich sediments. *Marine Geology* 80 (3–4), 231–267.
- Grasby, S.E., Beauchamp, B., 2009. Latest Permian to Early Triassic basin-to-shelf anoxia in the Sverdrup Basin, Arctic Canada. *Chemical Geology* 264 (1–4), 232–246.
- Grice, K., Cao, C., Love, G.D., Böttcher, M.E., Twitchett, R.J., Grosjean, E., Summons, R.E., Turgeon, S.C., Dunning, W., Jin, Y., 2005. Photic zone euxinia during the Permian–Triassic superanoxic event. *Science* 307 (5710), 706–709.
- Grotzinger, J.P., Knoll, A.H., 1995. Anomalous carbonate precipitates: is the Precambrian the key to the Permian? *Palaios* 10 (6), 578–596.
- Grotzinger, J.P., Reed, J.F., 1983. Evidence for primary aragonite precipitation, lower Proterozoic (1.9 Ga) Rocknest dolomite, Wopmay orogen, northwest Canada. *Geology* 11 (12), 710–713.
- Groves, J.R., Altiner, D., Boyce, M.D., Craig, B.J., 2003. “Disaster oolites” in the Permian–Triassic boundary interval, Tauride Mountains (Turkey). Annual Meeting: Geological Society of America Abstracts with Programs, v. 35, p. 48.
- Guangxi Bureau of Geology Mineral Resources, 1972. Regional geological report of the People's Republic of China, Laibin map, 1:200,000 (in Chinese).
- Gulbrandsen, R.A., 1969. Physical and chemical factors in the formation of marine apatite. *Economic Geology* 64 (4), 365–382.
- Hallam, A., 1991. Why was there a delayed radiation after the end-Palaeozoic extinctions? *Historical Biology* 5 (2), 257–262.
- Hallam, A., Wignall, P.B., 1997. *Mass Extinctions and Their Aftermath*. Oxford University Press, Oxford, 320 pp.
- Heggie, D.T., Skyring, G.W., O'Brien, G.W., Reimers, C., Herczeg, A.L., Moriarty, D.J.W., Burnett, W.C., Milnes, A.R., 1990. Organic carbon cycling and modern phosphorite formation on the East Australian continental margin: an overview. In: Notholt, A.J.G. (Ed.), *Phosphorite Research and Development*. Geological Society of London Spec. Publ., London, pp. 87–117.
- Heller, P.L., Komar, P.D., Pevear, D.R., 1980. Transport processes in ooid genesis. *Journal of Sedimentary Research* 50 (3), 943–951.
- Hips, K., Haas, J., 2006. Calcimicrobial stromatolites at the Permian–Triassic boundary in a western Tethyan section, Bükk Mountains, Hungary. *Sedimentary Geology* 185 (3–4), 239–253.
- Horton, A., Ivimey-Cook, H.C., Harrison, R.K., Young, B.R., 1980. Phosphatic ooids in the Upper Lias (Lower Jurassic) of central England. *Journal of the Geological Society of London* 137 (6), 731–740.
- Hotinski, R.M., Bice, K.L., Kump, L.R., Najjar, R.G., Arthur, M.A., 2001. Ocean stagnation and end-Permian anoxia. *Geology* 29 (1), 7–10.
- Hou, L., Luo, D., Fu, D., Hu, S., Li, K., 1991. Triassic Sedimentary–Tectonic Evolution in Western Sichuan and Eastern Xizang Region. Geological Publishing House, Beijing, 220 pp. (in Chinese with English abstract).
- Husinec, A., Read, J.F., 2006. Transgressive oversized radial ooid facies in the Late Jurassic Adriatic Platform interior: low-energy precipitates from highly supersaturated hypersaline waters. *Geological Society of America Bulletin* 118 (5–6), 550–556.
- Isozaki, Y., 1997. Permo–Triassic boundary superanoxia and stratified superocean: records from lost deep sea. *Science* 276 (5310), 235–238.
- Isozaki, Y., Shimizu, N., Yao, J., Ji, Z., Matsuda, T., 2007. End-Permian extinction and volcanism-induced environmental stress: the Permian–Triassic boundary interval of lower-slope facies at Chaotian, south China. *Palaeogeography Palaeoclimatology Palaeoecology* 252 (1–2), 218–238.
- Jin, Z., 1997. Petrology and sedimentary environments of Permian, Moyang, Ludian County, Guizhou Province. In: Feng, Z., Yang, Y., Jin, Z., Li, S., Bao, Z. (Eds.), *Lithofacies Paleogeography of Permian of South China*. Petroleum University Press, Dongying, pp. 171–181.
- Kajiura, Y., Yamakita, S., Ishida, K., Ishiga, H., Imai, A., 1994. Development of a largely anoxic stratified ocean and its temporary massive mixing at the Permian/Triassic boundary supported by the sulfur isotopic record. *Palaeogeography Palaeoclimatology Palaeoecology* 111 (3–4), 367–379.
- Kamo, S.L., Czamanske, G.K., Amelin, Y., Fedorenko, V.A., Davis, D.W., Trofimov, V.R., 2003. Rapid eruption of Siberian flood-volcanic rocks and evidence for coincidence with the Permian–Triassic boundary and mass extinction at 251 Ma. *Earth and Planetary Science Letters* 214 (1–2), 75–91.
- Kempe, S., 1990. Alkalinity: the link between anaerobic basins and shallow water carbonates? *Naturwissenschaften* 77 (9), 426–427.
- Kershaw, S., Zhang, T., Lan, G., 1999. A ?microbialite carbonate crust at the Permian–Triassic boundary in South China, and its palaeoenvironmental significance. *Palaeogeography Palaeoclimatology Palaeoecology* 146 (1–4), 1–18.
- Kershaw, S., Li, Y., Crasquin-Soleau, S., Feng, Q., Mu, X., Collin, P.-Y., Reynolds, A., Guo, L., 2007. Earliest Triassic microbialites in the South China block and other areas: controls on their growth and distribution. *Facies* 53 (3), 409–425.
- Kershaw, S., Crasquin, S., Forel, M.B., Randon, C., Collin, P.-Y., Kosun, E., Richoz, S., Baud, A., 2010. Earliest Triassic microbialites in Çürük Dag, southern Turkey: composition, sequences and controls on formation. *Sedimentology*. doi:10.1111/j.1365-3091.2010.01181.x.
- King, D.T., Chafetz, H.S., 1983. Tidal-flat to shallow-shelf deposits in the Cap Mountain Limestone Member of the Riley Formation, Upper Cambrian of central Texas. *Journal of Sedimentary Research* 53 (1), 261–273.
- Kinsman, D.J.J., 1969. Interpretation of Sr<sup>2+</sup> concentrations in carbonate minerals and rocks. *Journal of Sedimentary Research* 39 (2), 486–508.
- Knoll, A.H., Bambach, R.K., Canfield, D.E., Grotzinger, J.P., 1996. Comparative earth history and Late Permian mass extinction. *Science* 273 (5274), 452–457.
- Konhäuser, K., 2007. *Introduction to Geomicrobiology*. Blackwell Publishing, Oxford, 425 pp.
- Korte, C., Kozur, H.W., 2010. Carbon-isotope stratigraphy across the Permian–Triassic boundary: a review. *Journal of Asian Earth Sciences* 39 (4), 215–235.

- Korte, C., Kozur, H.W., Veizer, J., 2005.  $\delta^{13}\text{C}$  and  $\delta^{18}\text{O}$  values of Triassic brachiopods and carbonate rocks as proxies for coeval seawater and palaeotemperature. *Palaeogeography Palaeoclimatology Palaeoecology* 226 (3–4), 287–306.
- Kraimer, K., Vachard, D., 2009. The Lower Triassic Werfen Formation of the Karawanken Mountains (Southern Austria) and its disaster survivor microfossils, with emphasis on *Postcladella* n. gen. (Foraminifera, Miliolata, Cornuspirida). *Revue de Micropaléontologie*. doi:10.1016/j.revmic.2008.11.001.
- Krajewski, K.P., Van Cappellen, P., Trichet, J., Kuhn, O., Lucas, J., Martín-Algarra, A., Prévôt, L., Tewari, V.C., Gaspar, L., Knight, R.L., Lamboy, M., 1994. Biological processes and apatite formation in sedimentary environments. In: Föllmi, K.B. (Ed.), *Concepts and Controversies in Phosphogenesis*. *Eclogae Geologicae Helveticae*, pp. 701–745.
- Krajewski, K.P., Leśniak, P.M., Łacka, B., Zawadzki, P., 2000. Origin of phosphatic stromatolites in the Upper Cretaceous condensed sequence of the Polish Jura Chain. *Sedimentary Geology* 136 (1–2), 89–112.
- Krom, M.D., Berner, R.A., 1980. Adsorption of phosphate in anoxic marine sediments. *Limnology and Oceanography* 25 (5), 797–806.
- Kump, L.R., Pavlov, A., Arthur, M.A., 2005. Massive release of hydrogen sulfide to the surface ocean and atmosphere during intervals of oceanic anoxia. *Geology* 33 (5), 397–400.
- Lehrmann, D.J., 1993. Sedimentary geology of the Great Bank of Guizhou: Birth, evolution and death of a Triassic isolated carbonate platform, Guizhou Province, south China. PhD Thesis, University of Kansas, Kansas, 457 pp.
- Lehrmann, D.J., 1999. Early Triassic calcimicrobial mounds and biostromes of the Nanpanjiang basin, south China. *Geology* 27 (4), 359–362.
- Lehrmann, D.J., Enos, P., Payne, J.L., Montgomery, P., Wei, J., Yu, Y., Xiao, J., Orchard, M.J., 2005. Permian and Triassic depositional history of the Yangtze platform and Great Bank of Guizhou in the Nanpanjiang basin of Guizhou and Guangxi, south China. *Albertiana* 33, 147–166.
- Lehrmann, D.J., Ramezani, J., Bowring, S.A., Martin, M.W., Montgomery, P., Enos, P., Payne, J.L., Orchard, M.J., Wang, H., Wei, J., 2006. Timing of recovery from the end-Permian extinction: geochronologic and biostratigraphic constraints from south China. *Geology* 34 (12), 1053–1056.
- Lehrmann, D.J., Payne, J.L., Pei, D., Enos, P., Druke, D., Steffen, K., Zhang, J., Wei, J., Orchard, M.J., Ellwood, B., 2007. Record of the end-Permian extinction and Triassic biotic recovery in the Chongzuo–Pingguo platform, southern Nanpanjiang basin, Guangxi, south China. *Palaeogeography Palaeoclimatology Palaeoecology* 252 (1–2), 200–217.
- Li, F., Wang, X., Xue, W., Yan, J., 2010. Origin and environmental significance of giant ooids in the Early Triassic: a new kind of anachronistic facies. *Acta Sedimentologica Sinica* 28 (3), 48–58 (in Chinese with English abstract).
- Liu, J., Ezaki, Y., Yang, S., Wang, H., Adachi, N., 2007. Age and sedimentology of microbialites after the end-Permian mass extinction in Luodian, Guizhou Province. *Journal of Palaeogeography* 9 (5), 473–486 (in Chinese with English abstract).
- Markello, J.R., Read, J.F., 1981. Carbonate ramp-to-deeper shelf transitions of an Upper Cambrian intrashelf basin, Nolichucky Formation, Southwest Virginia Appalachians. *Sedimentology* 28 (4), 573–597.
- Mary, M., Woods, A.D., 2008. Stromatolites of the Lower Triassic Union Wash Formation, CA: evidence for continued post-extinction environmental stress in western North America through the Spathian. *Palaeogeography Palaeoclimatology Palaeoecology* 261 (1–2), 78–86.
- Mata, S.A., Bottjer, D.J., 2009. The paleoenvironmental distribution of Phanerozoic wrinkle structures. *Earth-Science Reviews* 96 (3), 181–195.
- McClellan, G.H., Van Kauwenbergh, S.J., 1990. Mineralogy of sedimentary apatites. In: Notholt, A.J.G. (Ed.), *Phosphorite Research and Development*. Geological Society of London Spec. Publ., London, pp. 23–31.
- McCrea, J.M., 1950. On the isotopic chemistry of carbonates and a paleotemperature scale. *Journal of Chemical Physics* 18 (6), 849–857.
- Mei, M., 2008. Implication for the unusual giant oolites of the Phanerozoic and their morphological diversity: a case study from the Triassic Daye Formation at the Lichuan section in Hubei Province, South China. *Geoscience* 22 (5), 683–698 (in Chinese with English abstract).
- Mundil, R., Ludwig, K.R., Metcalfe, I., Renne, P.R., 2004. Age and timing of the Permian mass extinctions: U/Pb dating of closed-system zircons. *Science* 305 (5691), 1760–1763.
- Nelson, G.J., Pufahl, P.K., Hiatt, E.E., 2010. Paleoclimatographic constraints on Precambrian phosphorite accumulation, Baraga Group, Michigan, USA. *Sedimentary Geology* 226 (1–4), 9–21.
- O'Brien, G.W., Milnes, A.R., Veeh, H.H., Heggie, D.T., Riggs, S.R., Cullen, D.J., Marshall, J.F., Cook, P.J., 1990. Sedimentation dynamics and redox iron-cycling: controlling factors for the apatite–glaucconite association on the East Australian continental margin. In: Notholt, A.J.G. (Ed.), *Phosphorite Research and Development*. Geological Society of London Spec. Publ., London, pp. 61–86.
- Opdyke, B.N., Wilkinson, B.H., 1993. Carbonate mineral saturation state and cratonic limestone accumulation. *American Journal of Science* 293 (3), 217–234.
- Payne, J.L., Kump, L.R., 2007. Evidence for recurrent Early Triassic massive volcanism from quantitative interpretation of carbon isotope fluctuations. *Earth and Planetary Science Letters* 256 (1–2), 264–277.
- Payne, J.L., Lehrmann, D.J., Wei, J., Orchard, M.J., Schrag, D.P., Knoll, A.H., 2004. Large perturbations of the carbon cycle during recovery from the end-Permian extinction. *Science* 305 (5683), 506–509.
- Payne, J.L., Lehrmann, D.J., Wei, J., Knoll, A.H., 2006a. The pattern and timing of biotic recovery from the end-Permian extinction on the Great Bank of Guizhou, Guizhou Province, China. *Palaios* 21 (1), 63–85.
- Payne, J.L., Lehrmann, D.J., Christensen, S., Wei, J., Knoll, A.H., 2006b. Environmental and biological controls on the initiation and growth of a Middle Triassic (Anisian) reef complex on the Great Bank of Guizhou, Guizhou Province, China. *Palaios* 21 (4), 325–343.
- Payne, J.L., Lehrmann, D.J., Follett, D., Seibel, M., Kump, L.R., Riccardi, A., Altiner, D., Sano, H., Wei, J., 2007. Erosional truncation of uppermost Permian shallow-marine carbonates and implications for Permian–Triassic boundary events. *Geological Society of America Bulletin* 119 (7–8), 771–784.
- Plee, K., Ariztegui, D., Martini, R., Davaud, E., 2008. Unravelling the microbial role in ooid formation – results of an in situ experiment in modern freshwater Lake Geneva in Switzerland. *Geobiology* 6 (4), 341–350.
- Posenato, R., 2008. Global correlations of mid Early Triassic events: the Induan/Olenekian boundary in the Dolomites (Italy). *Earth-Science Reviews* 91 (1–4), 93–105.
- Pruss, S.B., Bottjer, D.J., 2004. Late Early Triassic microbial reefs of the western United States: a description and model for their deposition in the aftermath of the end-Permian mass extinction. *Palaeogeography Palaeoclimatology Palaeoecology* 211 (1–2), 127–137.
- Pruss, S.B., Fraiser, M.L., Bottjer, D.J., 2004. Proliferation of Early Triassic wrinkle structures: implications for environmental stress following the end-Permian mass extinction. *Geology* 32 (5), 461–464.
- Pruss, S.B., Corsetti, F.A., Bottjer, D.J., 2005. Environmental trends of Early Triassic bio-fabrics: implications for understanding the aftermath of the end-Permian mass extinction. In: Over, D.J., Morrow, J.R., Wignall, P.B. (Eds.), *Understanding Late Devonian and Permian–Triassic Biotic and Climatic Events: Towards and Integrated Approach*. Elsevier, Amsterdam, pp. 313–332.
- Pruss, S.B., Bottjer, D.J., Corsetti, F.A., Baud, A., 2006. A global marine sedimentary response to the end-Permian mass extinction: examples from southern Turkey and the western United States. *Earth-Science Reviews* 78 (3–4), 193–206.
- Pufahl, P.K., Grimm, K.A., 2003. Coated phosphate grains: proxy for physical, chemical, and ecological changes in seawater. *Geology* 31 (9), 801–804.
- Qian, M., Fan, H., 1994. The stromatolite bioherms in the Lower Qinglong Fm. in Songshan, Wuxi and their environment. *Jiangsu Geology* 18 (1), 19–24 (in Chinese with English abstract).
- Regional Geological Survey of Sichuan Bureau of Geology and Nanjing Institute of Geology and Palaeontology, 1982. *Stratigraphy and Palaeontology in W. Sichuan and E. Xizang, China 1*. Sichuan Science and Technology Publishing House, Chengdu, 341 pp. (in Chinese with English abstract).
- Reolid, M., Gaillard, C., Lathuilière, B., 2007. Microfacies, microtaphonomic traits and foraminiferal assemblages from Upper Jurassic oolitic-coral limestones: stratigraphic fluctuations in a shallowing-upward sequence (French Jura, Middle Oxfordian). *Facies* 53 (4), 553–574.
- Richoz, S., Baud, A., Krystyn, L., Twichett, R., 2005. Permo–Triassic deposits of the Oman mountains: from basin and slope to the shallow platform. The 24th IAS Regional Meeting & Post-conference Excursion No. A13 in the Oman Mountains. Field Guidebook, Muscat, 58 pp.
- Richoz, S., Krystyn, L., Baud, A., Brandner, R., Horacek, M., Mohtat-Aghai, P., 2010. Permian–Triassic boundary interval in the Middle East (Iran and O. Oman): progressive environmental change from detailed carbonate carbon isotope marine curve and sedimentary evolution. *Journal of Asian Earth Sciences* 39 (4), 236–253.
- Richter, D.K., 1983. Calcareous ooids: a synopsis. In: Peryt, T.M. (Ed.), *Coated Grains*. Springer-Verlag, Berlin, pp. 71–99.
- Ruttenberg, K.C., Berner, R.A., 1993. Authigenic apatite formation and burial in sediments from non-upwelling, continental margin environments. *Geochimica et Cosmochimica Acta* 57 (5), 991–1007.
- Sandberg, P.A., 1983. An oscillating trend in Phanerozoic non-skeletal carbonate mineralogy. *Nature* 305 (5929), 19–22.
- Schubert, J.K., Bottjer, D.J., 1992. Early Triassic stromatolites as post-mass extinction disaster forms. *Geology* 20 (10), 883–886.
- Sepkoski, J.J., Bambach, R.K., Droser, M.L., 1991. Secular changes in Phanerozoic event bedding and the biological overprint. In: Eisele, G., Ricken, W., Seilacher, A. (Eds.), *Cycles and Events in Stratigraphy*. Springer-Verlag, Berlin, pp. 298–312.
- Siewers, F.D., 2003. Oolite and coated grains. In: Middleton, G.V. (Ed.), *Encyclopedia of Sediments and Sedimentary Rocks*. Kluwer Academic Publishers, Dordrecht, pp. 502–506.
- Simone, L., 1981. Ooids: a review. *Earth-Science Reviews* 16 (4), 319–355.
- Simonson, B.M., Schubel, K.A., Hassler, S.W., 1993. Carbonate sedimentology of the early Precambrian Hamersley Group of Western Australia. *Precambrian Research* 60 (1–4), 287–335.
- Singh, U., 1987. Ooids and cements from the Late Precambrian of the Flinders Ranges, South Australia. *Journal of Sedimentary Research* 57 (1), 117–127.
- Soudry, D., 2000. Microbial phosphate sediment. In: Riding, R.E., Awramik, S.M. (Eds.), *Microbial Sediments*. Springer-Verlag, Berlin, pp. 127–136.
- Soudry, D., Southgate, P.N., 1989. Ultrastructure of a Middle Cambrian primary nonpelletal phosphorite and its early transformation into phosphate vadoids: Georgina Basin, Australia. *Journal of Sedimentary Research* 59 (1), 53–64.
- Stanley, S.M., Yang, X., 1994. A double mass extinction at the end of the Paleozoic Era. *Science* 266 (5189), 1340–1344.
- Sumner, D.Y., 1997. Carbonate precipitation and oxygen stratification in late Archean seawater as deduced from facies and stratigraphy of the Gamohaan and Frisco Formations, Transvaal Supergroup, South Africa. *American Journal of Science* 297, 455–487.
- Sumner, D.Y., Grotzinger, J.P., 1993. Numerical modeling of ooid size and the problem of Neoproterozoic giant ooids. *Journal of Sedimentary Research* 63 (5), 974–982.
- Sun, S., Li, J., Chen, H., Peng, H., Hsu, K.J., Shelton, J.W., 1989. Mesozoic and Cenozoic sedimentary history of South China. *AAPG Bulletin* 73 (10), 1247–1269.
- Swett, K., Knoll, A.H., 1989. Marine pisolites from Upper Proterozoic carbonates of East Greenland and Spitsbergen. *Sedimentology* 36 (1), 75–93.
- Tang, B., 1987. The petrological features and sedimentary environment of carbonate rocks of the upper member of the Lower Qinglong Formation, Songshan, Wuxi. *Geological Review* 33 (5), 437–442 (in Chinese with English abstract).

- Teitz, M.W., Mountjoy, E.W., 1988. The Late Proterozoic Yellowhead carbonate platform west of Jasper, Alberta. In: Geldsetzer, H.H.J., James, N.P., Tebbutt, G.E. (Eds.), *Reefs, Canada and Adjacent Area: Canadian Society of Petroleum Geologists Memoir*, 13, pp. 129–134.
- Tian, J., Zeng, Y., 1995. The revolution of the isotopic composition of strontium in the Permian paleo-ocean in South China. *Acta Sedimentologica Sinica* 13 (4), 125–130 (in Chinese with English abstract).
- Trower, E.J., Grotzinger, J.P., 2010. Sedimentology, diagenesis, and stratigraphic occurrence of giant ooids in the Ediacaran Rainstorm Member, Johnnie Formation, Death Valley region, California. *Precambrian Research* 180 (1–2), 113–124.
- Truswell, J.F., Eriksson, K.A., 1973. Stromatolitic associations and their palaeo-environmental significance: a re-appraisal of a lower Proterozoic locality from the northern Cape province, South Africa. *Sedimentary Geology* 10 (1), 1–23.
- Tucker, M.E., 1984. Calcitic, aragonitic and mixed calcitic–aragonitic ooids from the mid-Proterozoic Belt Supergroup, Montana. *Sedimentology* 31 (5), 627–644.
- Tucker, M.E., 1985. Calcitized aragonite ooids and cements from the late Precambrian Biri Formation of Southern Norway. *Sedimentary Geology* 43 (1–4), 67–84.
- Van Cappellen, P., Berner, R.A., 1991. Fluorapatite crystal growth from modified seawater solutions. *Geochimica et Cosmochimica Acta* 55 (5), 1219–1234.
- Veizer, J., 1983. Trace elements and isotopes in sedimentary carbonates. *Reviews in Mineralogy and Geochemistry* 11 (1), 265–299.
- Veizer, J., Lemieux, J., Jones, B., Gibling, M.R., Savelle, J., 1977. Sodium: paleosalinity indicator in ancient carbonate rocks. *Geology* 5 (3), 177–179.
- Veizer, J., Ala, D., Azmy, K., Bruckschen, P., Buhl, D., Bruhn, F., Carden, G.A.F., Diener, A., Ebner, S., Godderis, Y., Jasper, T., Korte, C., Pawellek, F., Podlaha, O.G., Strauss, H., 1999.  $^{87}\text{Sr}/^{86}\text{Sr}$ ,  $\delta^{13}\text{C}$  and  $\delta^{18}\text{O}$  evolution of Phanerozoic seawater. *Chemical Geology* 161 (1–3), 59–88.
- Wang, S., Zhang, H., Peng, C., Chen, M., 2005. Strata of Palaeozoic–Mesozoic and Evolution of the Chasmic Furrow in Western Guizhou Province. Geological Publishing House, Beijing. 146 pp. (in Chinese with English abstract).
- Wang, Q., Tong, J., Song, H., Yang, H., 2009. Ecological evolution across the Permian/Triassic boundary at the Kangjiaping Section in Cili County, Hunan Province, China. *Science in China Series D Earth Sciences* 52 (6), 797–806.
- Weidlich, O., 2007. PTB mass extinction and earliest Triassic recovery overlooked? New evidence for a marine origin of Lower Triassic mixed carbonate–siliciclastic sediments (Rogenstein Member), Germany. *Palaeogeography Palaeoclimatology Palaeoecology* 252 (1–2), 259–269.
- Weidlich, O., 2010. Meteoric diagenesis in carbonates below karst unconformities; heterogeneity and control factors. In: van Buchem, F.S.P., Gerdes, K.D., Esteban, M. (Eds.), *Mesozoic and Cenozoic carbonate systems of the Mediterranean and the Middle East: Stratigraphic and Diagenetic Reference Models*. Geological Society of London Spec. Publ., London, pp. 291–315.
- Wignall, P.B., Twitchett, R.J., 1996. Oceanic anoxia and the End Permian mass extinction. *Science* 272 (5265), 1155–1158.
- Wignall, P.B., Twitchett, R.J., 1999. Unusual intraclastic limestones in Lower Triassic carbonates and their bearing on the aftermath of the end-Permian mass extinction. *Sedimentology* 46 (2), 303–316.
- Wilkinson, B.H., Buczynski, C., Owen, R.M., 1984. Chemical control of carbonate phases: implications from Upper Pennsylvanian calcite–aragonite ooids of southeastern Kansas. *Journal of Sedimentary Research* 54 (3), 932–947.
- Wilkinson, B.H., Owen, R.M., Carroll, A.R., 1985. Submarine hydrothermal weathering, global eustasy, and carbonate polymorphism in Phanerozoic marine oolites. *Journal of Sedimentary Research* 55 (2), 171–183.
- Woods, A.D., Bottjer, D.J., Mutti, M., Morrison, J., 1999. Lower Triassic large sea-floor carbonate cements: their origin and a mechanism for the prolonged biotic recovery from the end-Permian mass extinction. *Geology* 27 (7), 645–648.
- Woods, A.D., Bottjer, D.J., Corsetti, F.A., 2007. Calcium carbonate seafloor precipitates from the outer shelf to slope facies of the Lower Triassic (Smithian–Spathian) Union Wash Formation, California, USA: sedimentology and palaeobiologic significance. *Palaeogeography Palaeoclimatology Palaeoecology* 252 (1–2), 281–290.
- Wu, Y., Zhu, H., Zhu, Z., Yan, Y., 1994. Triassic Lithofacies, Paleogeography and Mineralization in South China. Geological Publishing House, Beijing. 143 pp. (in Chinese with English abstract).
- Xie, S., Pancost, R.D., Yin, H., Wang, H., Evershed, R.P., 2005. Two episodes of microbial change coupled with Permo/Triassic faunal mass extinction. *Nature* 434 (7032), 494–497.
- Xie, S., Pancost, R.D., Wang, Y., Yang, H., Wignall, P.B., Luo, G., Jia, C., Chen, L., 2010. Cyanobacterial blooms tied to volcanism during the 5 m.y. Permo–Triassic biotic crisis. *Geology* 38 (5), 447–450.
- Yang, H., Chen, Z.Q., Wang, Y., Tong, J., Song, H., Chen, J., 2011. Composition and structure of microbialite ecosystems following the end-Permian mass extinction in South China. *Palaeogeography Palaeoclimatology Palaeoecology* 308 (1–2), 111–128.
- Yin, H., Zhang, K., Tong, J., Yang, Z., Wu, S., 2001. The global stratotype section and point (GSSP) of the Permian–Triassic boundary. *Episodes* 24 (2), 102–114.
- Zempolich, W.G., Wilkinson, B.H., Lohmann, K.C., 1988. Diagenesis of late Proterozoic carbonates: the Beck Spring Dolomite of eastern California. *Journal of Sedimentary Research* 58 (4), 656–672.
- Zenger, D.H., 1976. Dolomitization and dolomite “dikes” in the Wyman Formation (Precambrian), northeastern Inyo Mountains, California. *Journal of Sedimentary Research* 46 (3), 457–462.
- Zhu, Z., 1992. Triassic megabeach on the southeastern margin of the Yangtze plate. In: Liu, B., Zeng, Y. (Eds.), *Collected Papers on Lithofacies and Paleogeography*. Geological Publishing House, Beijing, pp. 113–121.
- Zhu, H., Gu, R., Zhu, P., Cao, Z., Zhou, H., 1986. Characteristics of sedimentation and reservoirs of Qinglong Group, Triassic, southern Jiangsu Province. In: Liu, B., Zeng, Y. (Eds.), *Collected Papers on Lithofacies and Paleogeography*. Geological Publishing House, Beijing, pp. 31–52.
- Zhu, T., Li, Z., Li, C., Feng, X., Zhang, Q., Zhang, H., Lin, S., Zeng, Q., 2005. New data of Triassic strata in the Shuanghu area, northern Tibet, China. *Geological Bulletin of China* 24 (12), 1127–1134 (in Chinese with English abstract).